Inês Filipa de Oliveira Almeida

Licenciada em Bioquímica

Fighting breast cancer using membrane-active peptides

Dissertação para obtenção do Grau de Mestre em
Mestrado em Bioquímica

Orientador: Professor Doutor Miguel Castanho IMM/FM/UL
Co-orientadora: Doutora Diana Gaspar IMM/FM/UL

Presidente: Prof. Doutor Pedro Tavares
Arguente: Doutora Ana Magalhães
Vogal: Prof. Doutor Miguel Castanho

FACULDADE DE CIÊNCIAS E TECNOLOGIA
UNIVERSIDADE NOVA DE LISBOA

Setembro 2015

Inês Filipa de Oliveira Almeida

Licenciada em Bioquímica

Fighting breast cancer using membrane-active peptides

Dissertação para obtenção do Grau de Mestre em
Mestrado em Bioquímica

Orientador: Professor Doutor Miguel Castanho IMM/FM/UL
Co-orientadora: Doutora Diana Gaspar IMM/FM/UL

Presidente: Prof. Doutor Pedro Tavares
Arguente: Doutora Ana Magalhães
Vogal: Prof. Doutor Miguel Castanho

Setembro 2015

Fighting breast cancer using membrane-active peptides

Agradecimentos

Em primeiro lugar gostaria de agradecer ao professor Miguel Castanho, pela oportunidade de fazer parte de uma equipa de excelência como a sua e pela forma como sempre me acolheu no seu laboratório.

À Diana Gaspar um enorme obrigada por todo o tempo dedicado e por tudo aquilo que me ensinou, tanto a nível científico como pessoal. Obrigada por me ter ajudado a crescer a todos os níveis neste último ano.

A todos os elementos da unidade MCastanho, de um modo especial à Susana pela grande amiga, companheira, ouvinte e conselheira que se revelou, tenho consciência que sem a sua presença tinha sido mais difícil. Ao Tiago, por ter sempre uma palavra de incentivo, um conselho ou um simples sorriso logo pela manhã. À Liliana por estar sempre presente, pela sua prontidão em ajudar, por tudo aquilo que me ensinou e pela amizade.

Um enorme obrigado a todos os amigos FCTenses que mesmo longe estiveram sempre presentes com uma palavra de incentivo ou com um simples abraço (muitas vezes virtual), de um modo especial à Inês, ao João, à Ana, à Mariana e à Aline. À "família" com quem tive a honra de viver durante os tempos de faculdade e que, apesar da minha ausência neste último ano, nunca permitiram que deixasse de partilhar das vossas aventuras; obrigada pela vossa amizade sem fim.

Aos meus amigos de sempre que são essenciais no que toca a "recarregar baterias", em especial à Rita por estar sempre presente.

Por último, obrigada à minha família por estar sempre lá quando mais preciso… Ao meu irmão que tem sido muito mais que um braço direito, a todos os níveis, no meu percurso académico. Aos meus pais, pelo apoio incondicional, pelo esforço que fazem diariamente para que tudo isto seja possível e pela força e coragem que sempre me transmitiram.

Mais uma vez, a todos, os meus mais sinceros agradecimentos.

Resumo

O cancro continua a ser uma das principais causas de mortalidade. As terapias existentes apresentam limitações que contribuem para uma reduzida taxa de sucesso no tratamento. Uma alternativa promissora a este problema consiste na possibilidade de utilizar péptidos antimicrobianos (AMPs) no combate ao cancro.

Este trabalho teve como objetivos avaliar a capacidade citotóxica de três AMPs contra células de cancro de mama, a seletividade relativamente a células saudáveis e ainda compreender o mecanismo de ação.

Por determinação da citotoxicidade dos péptidos (pepR, HNP-1 e PvD1), recorrendo à redução do sal de tetrazólio MTT, na presença de cada linha celular (MDA-MB-231 e MCF 10A) verificou-se que tanto o pepR como o PvD1 são seletivos a células cancerígenas, requerem menor concentração para inibir 50% da população (IC_{50}), comparativamente às saudáveis. Contrariamente, o HNP-1 não mostrou ser um péptido anticancerígeno (ACP) promissor dado que induz a morte celular de igual forma para ambas as linhas celulares.

Realizaram-se estudos de potencial-zeta para avaliar alterações à superfície das células induzidas por interações péptido-célula. Contrariamente ao descrito quando atuam como AMPs, pepR e HNP-1 não requerem neutralização da superfície celular.

Com base nos resultados anteriores, o PvD1 revelou-se o mais promissor dos péptidos e consequentemente estudou-se a sua ação por microscopia de força atómica (AFM). Esta técnica permitiu avaliar os perfis de altura bem como a rugosidade da superfície celular quando submetida a diferentes concentrações de PvD1. Observou-se que não ocorrem alterações significativas da altura das células associadas ao aumento da concentração de péptido. Por outro lado, ao avaliar a rugosidade nas diferentes regiões celulares verifica-se que em algumas delas surgem alterações associadas ao aumento de PvD1.

Embora não seja possível propor o mecanismo de ação para estes ACPs pode concluir-se que tanto o PvD1 como o pepR são promissores no combate do cancro de mama.

Palavras-chave: péptidos anticancerígenos; cancro de mama; carga superficial da membrana; microscopia de força atómica.

Abstract

Cancer is still one of the major death causes worldwide demanding an urgent search for new therapies that combine selectivity, efficacy and ability to avoid resistance by cancer cells. One of the biggest advances in anticancer therapy is the use of antimicrobial peptides' (AMPs) as chemotherapy drugs since some of them showed both antimicrobial activity and selective anticancer activity.

In this work, the anticancer activity of three different AMPs, pepR, HNP-1 and PvD1, was tested against cancer and non-tumorigenic breast cell lines (MDA-MB-231 and MCF 10A).

The cytotoxic activity of each peptide was evaluated by MTT tetrazolium assay and the determination of the half maximal inhibitory concentration (IC_{50}), and showed that pepR and PvD1 act as anticancer peptides (ACPs), able to select between cancer and non-tumorigenic cells, whereas HNP-1 is not a promising ACP once it is not selective, killing both cell lines at the same concentration. Then, zeta-potential was used to evaluate the peptide-cell interaction and its effect in cells' surface charge. In this case, surface neutralization is not required before cell death, contrary to what happens when these peptides act like AMPs.

Finally, according with previous results, PvD1 was chosen as the most promising peptide and, as such, used for imaging assays with atomic force microscopy (AFM). With this technique height profiles and surface roughness were evaluated for both cell lines in absence and presence of three different PvD1 concentrations. It was concluded that, with the increase of peptide concentration there are no significant changes in cell's height profiles. On the other hand, when analysed separately, nucleus and cytoplasm present surface roughness changes associated to the increasing of PvD1 concentration.

Although it is not yet possible to propose a mechanism of action, both pepR and PvD1 are efficient against MDA-MB-231 cells and selective to MCF 10A cells.

Keywords: Anticancer peptide; breast cancer; membrane surface charge; atomic force microscopy

1. Index

2. List of Figures

3. List of Tables

4. Abbreviations and Symbols

ε	Dielectric constant
Z	Zeta-potential
η	Viscosity
ACP	Anticancer peptide
AFM	Atomic Force Microscopy
AMP	Antimicrobial peptide
ATCC	American Type Culture Collection
ATP	Adenosine triphosphate
BCEC	Brain Capillary Endothelial Cells
BPE	Bovine Pituitary Extract
DMEM	Dulbecco's Modified Eagle Medium
DMSO	Dimethyl sulfoxide
f (κa)	Henry's function
FBS	Fetal Bovine Serum
HUVEC	Human Umbilical Vein Endothelial Cells
IC_{50}	Half maximal inhibitory concentration
MCF7	Human breast cancer cells
MCF 10A	Non-tumorigenic breast cells
MDA-MB-231	Human breast cancer cells
MEBM	Mammary Epithelial Basal Medium
MOLT-4	Human acute lymphoblastic leukaemia
MTS	3-(4,5-dimethylthiazol-2-yl)-5-(3-carboxymethoxyphenyl)-2-(4-sulfophenyl)-2H-tetrazolium
MTT	3-(4,5-dimethylthiazol-2-yl)-2,5-diphenyltetrazolium bromide

M_W	Molecular weight
NADH	Nicotinamide adenine dinucleotide
NADPH	Nicotinamide adenine dinucleotide phosphate
OSCC	Oral squamous cell carcinoma
PBS	Phosphate Buffered Saline
PC	Phosphatidylcholine
PC-3	Human prostate adenocarcinoma
PE	Phosphatidylethanolamine
PI	Phosphatidylinositol
PS	Phosphatidylserine
RBC	Red blood cells
RCC	Renal cell carcinomas
rhEGF	Epidermal Growth Factor human recombined
R_{ms}	Root-mean-square roughness
SM	Sphingomyelin
TFA	Trifluoroacetic acid
U_E	Electrophoretic mobility
UV	Ultraviolet
XTT	2,3-Bis-(2-Methoxy-4-Nitro-5-Sulfophenyl)-2H-Tetrazolium-5-Carboxanilide
WST-1	2-(4-Iodophenyl)-3-(4-nitrophenyl)-5-(2,4-disulfophenyl)-2H-tetrazolium

1. Introduction

Cancer is still among the leading causes of mortality and morbidity around the world [1]. Despite numerous recent advances in treatment alternatives, the number of cancer cases is increasing as a result of aging, population growth and the increasing of some lifestyle choices such as smoking and physical inactivity. Breast and lung cancers are the most common diagnosis in females and males, respectively [2]–[4]. Although, “cancer” refers, in fact, to over 100 different diseases, all of their forms are commonly described as an abnormal cell growth which is able to invade other tissues and form a tumour mass, new vessels and spread through the body as metastasis [5], [6]. Surgery, chemotherapy and radiotherapy are the most used treatments against cancer, however, all of them present a low success rate and, reoccurrence risk [6], [7]. Chemotherapeutic agents are the most used treatment, especially, in case of advanced or metastatic disease [7]. However, there are many problems associated with this therapy as well as the inability to deliver the correct amount of drug directly to cancer cells (without affecting healthy cells and tissues) and, chemical resistance [4]–[6], [8]. Furthermore, chemotherapy is also responsible for some side-effects mainly induced in healthy cells which also divide rapidly, such as, decrease in production of blood cells (myelosuppression), inflammation of the digestive tract lining (mucositis) and hair loss (alopecia) [9]. In order to avoid drug resistance and all side effects associated to the currently used therapies many efforts have been made towards the development of a new class of anticancer drugs [2], [7], [9].

1.1. Antimicrobial peptides

Since the discovery of antiobiotics in 1930s that its inappropriate, excessive and irrational use has reduced their efficiency, induced increasing rates of antibiotics resistance and consequently became a public health problem worldwide [4], [10]–[12]. With the growing problem of resistance to conventional antibiotics, arises an urgent demand for novel antimicrobials and consequently the increasing interest in pharmacological applications of antimicrobial peptides (AMPs) as human therapeutics [6], [11], [13].

AMPs are produced by many organisms and are described as important components of innate host defence to prevent the infection by microbial pathogens [4], [14], [15]. In addition, more recently, these peptides have also been synthesized or produced by genetically engineered microorganisms in order to improve their bioavailability and stability, as well as reduce their amino acid sequences [13], [16]. AMPs are defined as being generally small and amphipathic molecules. Their sequence length ranges from 12 to 100 amino acid and is composed, in elevated proportion, by cationic and hydrophobic residues. The net charge of these peptides may vary from +2 to +9 however, values between +4 to +6 are the most common [4], [17].

According to their structure, AMPs can be classified into four groups: α-helical, β-sheet, extended and looped peptides [18]–[21]. The α-helical AMPs are usually unstructured in aqueous solution and, in membranes, form amphipathic helices. The β-sheet peptides are stabilized by two to four disulfide bonds, which form relatively rigid structures [20]. The extended AMPs have no regular secondary structure but are rich in specific amino acids such as proline, tryptophan arginine and/or histidine [19]. Finally, the loop peptides, as the name suggests, adopt a loop formation with only one disulfide bond [19], [20], [22].

The AMPs' ability to rapid and strongly interact with lipidic membranes through non-specific interactions, namely with microbial membranes, makes them promising candidates for a new generation of antibiotics free of microbial resistance. However, the capacity of disrupting and permeate cell's membrane is dependent on the biophysical properties, such as, amphipathicity, size, net charge and secondary structure [4], [14].

There are several mechanisms of action proposed to explain the AMPs' mode of action, but the first steps are common to all of them. Cationic AMPs starts to target the negatively charged microbe's membrane by an electrostatic interaction [6], [22]. This interaction has to continuously occur until it reaches the minimum concentration to be effective, named as threshold concentration, as shown in Figure 1.1 [21]. Once the threshold concentration is reached, one of the proposed mechanisms of action occurs. Some of these mechanisms are describe below [6], [21], [22].

The barrel-stave mechanism (Figure 1.1 a.) can be simply described as a transmembrane pore hydrophilic formation by AMPs. This mode of action involves four major steps. Peptides bind to the membrane's surface as monomers and changes its conformation to a transition phase, which the polar-phospholipid head groups induce localized membrane thinning. After that, the peptide's hydrophobic part is inserted into the membrane and the pore formation starts. Finally, the last step of this process consists in a continued recruitment of peptides to increase the pore size [22], [23].

In carpet mechanism (Figure 1.1 b.), as previously described, peptides adsorb to the membrane surface through electrostatic interactions, bind to the phospholipid head groups and start covering it in a carpet-like manner. After reaching the threshold concentration, AMPs insert and permeate the cell membranes inducing the loss of integrity or, in the case of continuous permeation, can leading to micellization [22]–[24].

As the carpet mechanism, the toroidal pore mechanism starts with peptides oriented parallel to the membrane (Figure 1.1 c.). The hydrophobic region of peptides start their entry in the hydrophobic core of the membrane leading to a local membrane curvature. At the threshold concentration the peptides change their orientation relative to the membrane becoming perpendicular and the continuity between inner and outer leaflets is established [6], [14], [21], [22].

Finally, the disordered toroidal pore mechanism is a recent modification of the previously presented toroidal pore mechanism (Figure 1.1 d.). As the name suggests, the pores formed are significantly more irregular than the previous model, the peptides are largely disordered and adopt different orientations. These features could contribute to a not well structured pore [21], [25], [26].

Besides their natural functions as part of the innate immune defence mechanism and their main application as a new generation of antibiotics, AMPs are also attracting attention as alternatives to food additives or anticancer drugs [13].

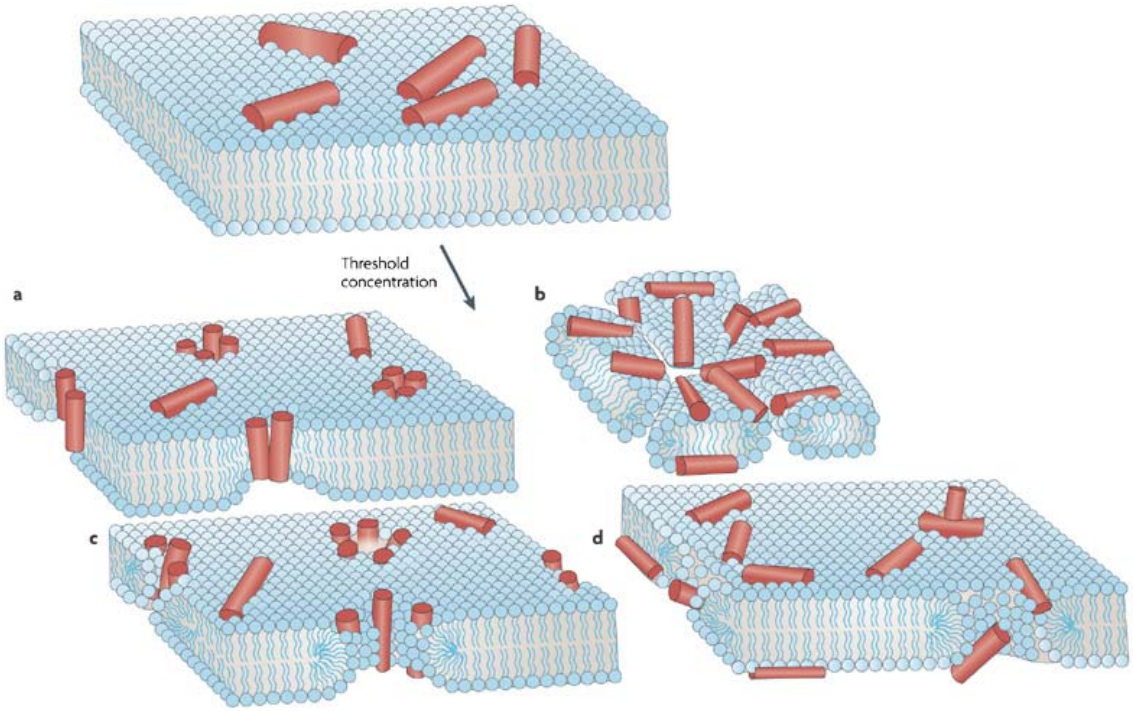

Figure 1.1 – Proposed mechanisms of membrane disruption by antimicrobial peptides (AMPs). **a.** Barrel-stave mechanism in which peptides enter perpendicularly to the membrane. **b.** Carpet mechanism, where the AMPs adsorb parallel to the outer leaflet which leads to membrane's loss of integrity. **c.** Toroidal pore mechanism is described initially as a carpet model but, after reaching the threshold concentration, AMPs change their orientation relative to the membrane establishing the continuity between inner and outer leaflets. Finally, the **d.** disordered toroidal mechanism is also described by the formation of a pore but in this case AMPs adopt different orientations that could contribute to a not well structured pore (From reference [21]).

1.2. Anticancer peptides

The increasing interest in AMPs as a new generation of antibiotics, arose. However, recent studies showed that a significant number of these peptides also exhibit cytotoxic activity against cancer cells [4], [6], [7]. This class of antimicrobial peptides is described as small molecules with an efficient tissue penetration and uptake by cancer cells [4], [7], [8]. As in AMPs, there are some proposed mechanisms of action that can be also applied to ACPs, namely carpet and barrel-stave models [4], [6].

Anticancer peptides can be classified into two major groups, peptides which are highly potent against bacteria and cancer cells but not to healthy mammalian cells, and peptides that are cytotoxic for bacteria, cancer and normal cells [4], [6], [24]. ACPs' ability to differentiate between cancer and healthy cells is still unknown but some authors propose that this selectivity is associated with both peptide characteristics and target membrane features [4], [27], [28].

1.3. pepR – a peptide from dengue virus

pepR (LKRWGTIKKSKAINVLRGFRKEIGRMLNILNRRRR – residues 67–100 of DENV-2 C protein) is a novel peptide with 35 amino acids, derived from the putative RNA-binding domain of the dengue virus' capsid protein [29], [30]. This peptide has a molecular weight of 4278.2 Da [30] and a positive charge of +12 (at pH 7.4) [29]. In water, pepR acquires a random coil conformation, whereas in membranes tend to form a single long α-helix [31] (Three dimensional (3D) structure represented in Figure 1.2).

This peptide was classified as an effective antimicrobial agent since it was able to inhibit *E. coli* growth even at micromolar concentrations [29]. Furthermore, the weak interaction of this peptide with zwitterionic lipids [32] could be a promising feature of peptide's selective ability between different cells.

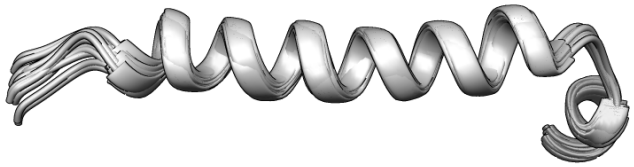

Figure 1.2 – 3D representation of pepR structure obtained from DENV C protein monomer (PDB code: 1R6R). The conformational representation was done with Chimera software.

1.4. HNP-1 – a human defensin

Defensins are one of the most characterized families of antimicrobial peptides found in different living organisms [33]. These peptides are an important component of innate immune system and are able to kill or eliminate a wide variety of fungi, enveloped virus, protozoans, Gram-negative and Gram-positive bacteria [33]–[35]. Furthermore, this family of AMPs also present different functions in numerous cellular processes such as cell division, wound healing, attraction and maturation of immune cells and differentiation and reorganization of epithelial tissues [34], [36].

Defensins are small peptides, positively charged at physiological pH with 29 to 45 amino acid residues. These AMPs have six conserved cystein residues (cys) which form three intramolecular dissulfide bridges and their molecular weight ranges from 3.5 to 6.5 kDa [6], [34]. The defensin family further comprises three sub-families, namely, α-, β- and θ-defensins [35], [37].

The Human Neutrophil Peptides (HNP 1-4) [34] are produced in azurophil granules of neutrophils and belong to the α-defensins sub-family [38], [39]. The HNP-1 (ACYCRIPACIAGERRYGTCIYQGRLWAFCC) [17], with 30 amino acid residues and a molecular weight of 3442 Da, is one of the most abundant and studied α-defensin. In solution, this peptide is arranged as a dimer and each monomer present a positive charge of +3 conferred by 4 arginine residues and a negative glutamic acid (3D structure represented in Figure 1.3) [17], [40]. With the increasing interest in these defensins some authors have concluded that HNP-1 may be expressed in order to modulate tumour progression, such as described by Müller et al [41] in renal cell carcinomas (RCC). Others authors confirm the cytotoxic effect against cancer cells [42], [43] whereas McKeown et al [39] already confirmed this effect in both oral squamous cell carcinoma (OSCC) and normal oral keratinocytes, showing that HNP-1 has no selectivity between cancer and healthy cells.

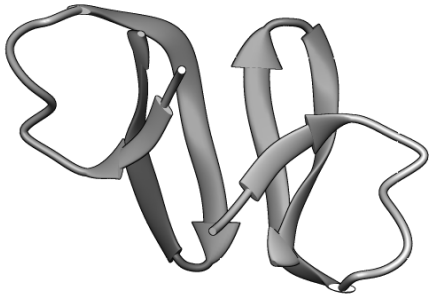

Figure 1.3 – 3D representation of HNP-1 monomer structure. The representation was done with Chimera software using the PDB code 3GNY.

1.5. PvD1 – a plant defensin

Like animals, plants also have AMPs as part of its innate immune system, defensins being the major constituent [44], [45]. Plant defensins have 45 to 54 amino acid residues, a positive charge, a molecular weight between 5 and 7 kDa [46] and commonly four disulfide bonds which are responsible for the stabilization of the 3D structure (three anti-parallel β-strands and one α-helix) [44], [47].

PvD1 defensin was isolated and purified from the seeds of common bean (*Phaseolus vulgaris*), originated in Central and South America [44], and although the complete amino acid sequence is not known, the antimicrobial activity of PvD1, especially antifungal activity, has been

confirmed [48]. According to Games et al [44] the molecular mass of PvD1 is approximately 6 kDa and was obtained by an SDS-Tricine gel electrophoresis.

1.6. From healthy to cancer cells

Although the human body is made of so many different organs, cell tissues can be divided in four main different categories according to their morphology: epithelial, connective, muscular or nervous tissues [49]. Cells of the epithelial tissue are characterized by being contiguous, joined by cell-to-cell junctions and organized as layers that cover the entire body and lining cavities, tubs and ducts. The cells that make up the muscular tissue are described by a large amount of contractile proteins in their cytoplasm, such as actin and myosin and are responsible for the movement of the whole body [49]. The nervous tissue is made up of neurons which are specialized in transmit and integrate electrical impulses to receive and process information, both from the inside and outside the body. The connective tissue is characterized by its extracellular matrix and underlies or supports the other three tissues previously described [49]. Epithelial tissue is the most important in this work once it is responsible for the most common human cancers, carcinoma [50].

The transformation process of healthy cells in cancer can be described as a multi-step process [50]. In the first step, an abnormal growth starts with only a minimal deviation from healthy cells, which is termed hyperplasia, when is induced by only one type of cells, or metaplasia, if the deviation is induced by cells of another type. The second step, named dysplasia, is when individual cells lose their normal appearance and cytological changes arise, such as variability in nucleus size and shape. The dysplastic tissue is described as a transition state between a benign and premalignant growth [50]. The third step is described by the formation of new types of tissue, both benign and malignant, and is termed neoplasia. In the last step of this transformation process, cancer cells acquire the ability of invade other tissues through the process of metastasis [50]. The metastases use the blood and lymph vessels to travel through the body and colonize new organs at distant sites [51].

Besides all transformation processes previously described, the most important difference between healthy and cancer cells focuses in plasma membranes. Healthy mammalian cells are mainly composed of zwitterionic phospholipids such as phosphatidylethanolamine (PE), phosphatidylcholine (PC) and sphingomyelin (SM). Additionally, these cells have high contents of cholesterol which acts as a protective molecule by altering the membrane fluidity, reducing membrane elasticity, blocking the entry of peptides and increasing their mechanical strength as well as their lipid packing [4], [6], [28], [52].

On the other hand, cancer cells' membrane, like in bacteria, are characterized by a slightly more negative charge than normal cells [4], [22], [53], [54] which is induced by the presence of phospholipids such as phosphatidylserine (PS), phosphatidylinositol (PI), phosphatidylglycerol

(PG) or cardiolipin (CL). Furthermore, the abundant microvilli and the low contents of cholesterol in cells' surface tends to increase the fluidity which, together with the cationicity of peptides, facilitate the electrostatic interactions between ACPs and cells membrane [4], [9], [28], [53].

There are different types of cell death which play an important role in several biological processes, among them stands out apoptosis and necrosis. Apoptosis is described as a programmed cell death that affects individual cells and is characterized by a decreasing in its volume, chromatin condensation, membrane blebbing and the formation of apoptotic bodies [55]. On the other hand, necrosis is an unprogrammed cell death that occurs due to extreme physiological conditions [55], [56]. It can be described by an increasing in cell volume, fragmentation of the chromatin and appearance of mitochondria with an aberrant morphology [55], [57], [58].

1.7. Cell viability

There are a variety of assay methods that can be used to estimate the metabolic activity of cells such as tetrazolium reduction, resazurin reduction and ATP detection [59]. Different tetrazolium compounds as 3-(4,5-dimethylthiazol-2-yl)-2,5-diphenyltetrazolium bromide (MTT), 3-(4,5-dimethylthiazol-2-yl)-5-(3-carboxymethoxyphenyl)-2-(4-sulfophenyl)-2H-tetrazolium (MTS), 2,3-Bis-(2-Methoxy-4-Nitro-5-Sulfophenyl)-2H-Tetrazolium-5-Carboxanilide (XTT) and 2-(4-Iodophenyl)-3-(4-nitrophenyl)-5-(2,4-disulfophenyl)-2H-tetrazolium (WST-1) have been commonly used [60]. In this case, a MTT tetrazolium reduction assay was used to evaluate the cytotoxicity of each peptide against human breast cells. Despite the variety of tetrazolium compounds, MTT was chosen since it can rapidly penetrate viable cells as well as can be metabolized by most cell types [59].

When metabolic active cells are in contact with MTT solution a reduction of a soluble tetrazolium into insoluble formazan crystals, by NADH or NADPH, occurs (Figure 1.4). The amount of formazan product formed (which is directly proportional to the number of viable cells) is quantified by absorbance reading. Nikkhah [61] concluded that the optimal wavelength for the formazan solution, in DMSO, is at 550 nm.

Initially, it was proposed that MTT is reduced only by active mitochondria in viable cells. However, later it was found that other cellular organelles were also able to reduced MTT [62]. Additionally, according to Liu [63], the subcellular fractions as nuclear, mitochondrial, microsomal and cytosolic can reduce MTT to formazan crystals in presence of NADH or NADPH. First the formazan product was deposited predominantly in a perinuclear region of the cytoplasm and then, with a longer incubation time, the insoluble product of MTT reduction also appears at the cell surface [61], [63].

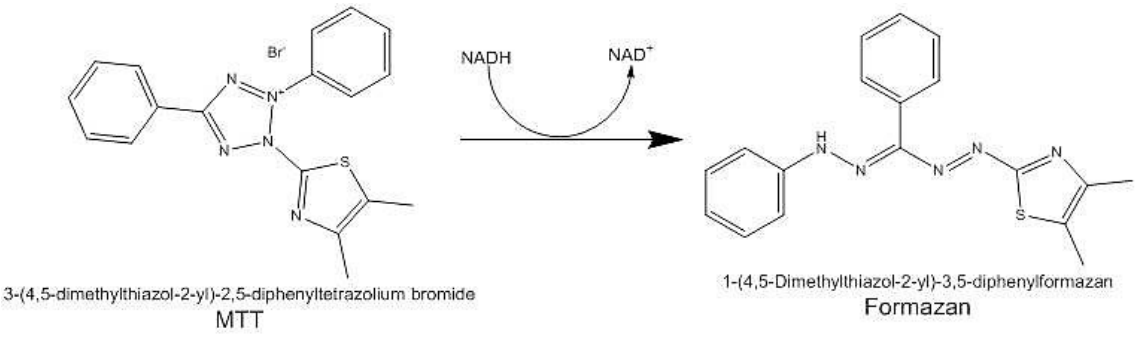

Figure 1.4 – Reduction of MTT tetrazolium into formazan crystals by NADH. Structures were obtained using ChemBioDraw software.

1.8. Zeta-Potential

Light-scattering techniques, such as static light scattering (SLS), dynamic light scattering (DLS) or zeta-potential, are non-invasive methods which enables studying the mechanisms of action of membrane active peptides at the molecular level. These techniques are useful as tools to determine size, average molecular weight (M_w), aggregation behaviour of peptides in solution (alone or with lipid membranes) and surface charge of particles in suspension in an aqueous environment [64].

Zeta-potential, the most recent light-scattering technique, could be described as a physical property exhibited by any particle in suspension [65]. As can be seen in Figure 1.5, a charged particle in suspension uses an electrostatic potential to attract ions with opposite charge to its surface producing a rearrangement of local free ions in solution and a strong bound ion layer which covers the particle's surface. This is commonly described as inner region or Stern layer. A second layer, outside the Stern layer, is also formed, which is given the name of outer region or diffuse layer and is described as a region where the ions are less firmly associated [64]. When an electric field is applied to the solution, charged particles are attracted to the electrode of the opposite charge inducing their movement. Consequently, ions strongly bound from Stern layer will move with it, whereas the ions present in the diffuse layer are not able to move with the particles and stay with the bulk dispersant. The zeta-potential corresponds to the potential formed at this boundary and can be calculated by the electrophoretic mobility [64], [65].

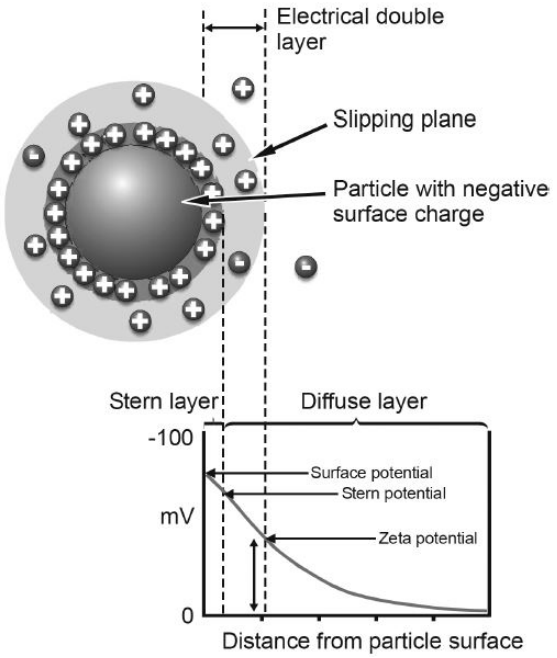

Figure 1.5 – Schematic representation of different layers surrounding a charged particle and the region where zeta-potential can be calculated (Adapted from [66]).

The zeta-potential of particles and their electrophoretic mobility are related by the Henry equation [64], [67]:

$$U_E = \frac{2\varepsilon z f(\kappa a)}{3\eta} \quad (1)$$

where U_E is the electrophoretic mobility, z the zeta-potential, ε the dielectric constant, η the viscosity and f(κa) the Henry's function. Henry's function value varies according to the media in which the particles lie. When the particles are suspended in aqueous solutions, according to Smoluchowski approximation, the f(κa) value is 1.5, whereas, if the particles are in a nonaqueous media (Huckel approximation) the value of this function is 1.

Despite the use of zeta-potential in so many applications already described as science and engineering, it is also a useful tool that could be applied in different industries like pharmaceutical or food, in order to for example, characterize particles' physical properties or biomedical polymers [65], [68].

1.9. Atomic Force Microscopy

In 1986 Binnig and Quate proposed a new method based on a different type of microscope able to investigate surfaces at the atomic scale which was named atomic force microscope (AFM) [69]. The atomic force microscope is very different from the other microscopies once the image is not obtained by focusing light or electrons on a surface as seen in optical or electron microscopy [70]. According to the Figure 1.6, a sensitive and flexible cantilever, with a sharp tip at the end, scans the surface of the sample and measures its interactions with the tip, in particular, measures the force between atoms from the sample and those of the tip [71]–[73]. On the opposite face of cantilever (relative to the tip) there is an incident laser which is reflected in a photodiode. A piezoelectric support is responsible for the movement of the cantilever on xy plane and, at the same time, allows z-axis movements by feedback. All the interactions between the tip and the samples will induce bending or twisting of the cantilever, proportional to the interaction force, which will vary the laser reflection point and hence the point of incidence in the photodiode. All the deflections are monitored during the scan and will be translated into a three-dimensional image of the height of the sample's surface [71]–[74].

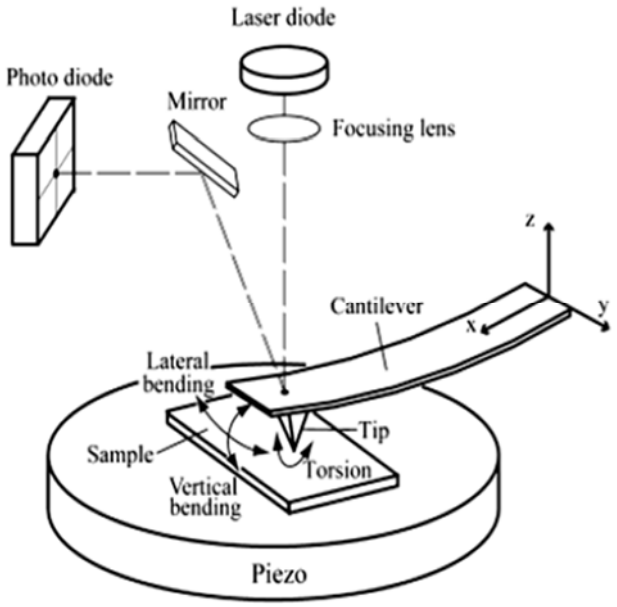

Figure 1.6 – Schematic representation of atomic force microscope (AFM) (From reference [75]).

The AFM has different imaging modes which are chosen depending on the application or the sample's nature. The most currently used are contact and tapping modes (Figure 1.7 a. and b. respectively). Contact mode, the older but frequently used, is described by a tip scanning the sample with a constant force usually between 10^{-7} and 10^{-12} N [71]. The biggest advantage of this mode is its higher resolution comparing with the other modes. On the other hand, there are some

limitations such as sample deformation during the scanning, sample damage caused by dragging of part of the sample or tip damage/change by scanning process [71], [73], [76].

The tapping (or intermittent) mode (Figure 1.7 b.) is more recent and also able to deliver high resolution images reducing the damages caused by the tip. The tapping mode imaging consists in oscillating the cantilever with a predefine frequency (typically at its resonant frequency), amplitude and height baseline. When the cantilever approaches to the surface sample, an interaction between them occurs and changes the oscillation parameters. This mechanism reduces the effects of friction or drag forces but have also limitations since it has proved more challenging when used in liquids and, comparing with contact mode, the scan's speed is slower [71], [76].

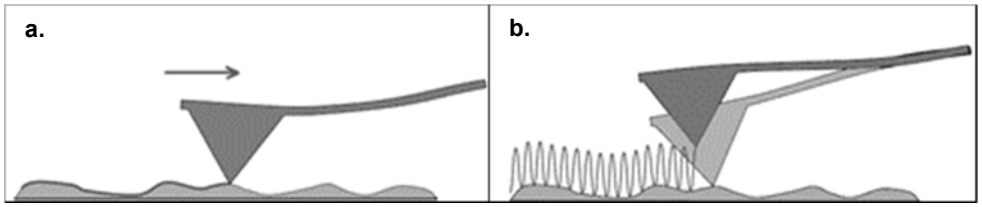

Figure 1.7 – Representation of the most currently used AFM imaging modes. **a.** Contact mode and **b.** tapping mode (Adapted from reference [77]).

As an improvement of sensitivity and specificity of molecular interaction, the tips can be modified (Figure 1.8 a. and b.). The tips that are functionalized with a specific chemical functional group, molecule or macromolecules enables measuring probe-sample forces as well as allows distinguish between sample's regions with different chemical structures and functionalities [78]. More recently, rather than tip, a living cell can be attached to the AFM cantilever (Figure 1.8 c.), allowing the study of cell-cell or cell-substrate interactions [79].

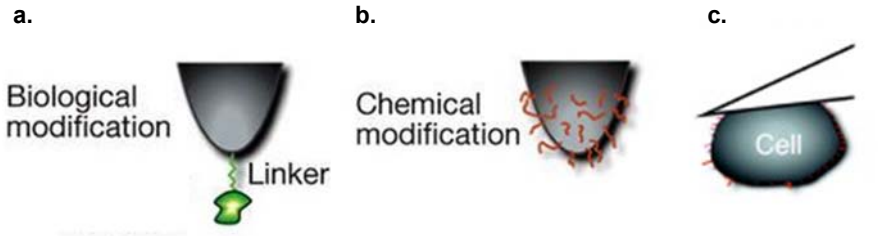

Figure 1.8 – Examples of AFM tip or cantilever functionalization to improve sensitivity and specificity. **a.** The biological modification is described by a tip functionalization with a biological molecule using a linker such as an antibody or a ligand. **b.** For chemical modification the AFM tip is directly functionalized with chemical groups. **c.** In the single-cell force spectroscopy the tip is replaced by a living cell which is attached to the AFM cantilever (Adapted from references [72], [80]).

About 90% of the AFM applications belong to different areas such as physics, nanotechnology, life sciences and industry, however, art conservation, food science or geology have also used AFM, although with less impact [81].

1.10. Objectives

The main goal of this work consists in evaluating the cytotoxic activity of three different AMPs against human breast cancer cells as well as their selectivity towards healthy and cancer cells. In addition, after proving their anticancer activity, the mechanism of action of these peptides when act as ACPs were evaluate.

In the first step of this work, the cytotoxic activity of each peptide against cancer and healthy cells was evaluated with a MTT tetrazolium assay. Then, the effect of each peptide in the surface charge membrane of both cell types was evaluated using zeta-potential techniques. The best among the three different anticancer peptides will be chosen and used for AFM imaging studies against both cell lines. The goal of these studies is to evaluate the effect induced by ACP on the cell's membrane surface.

2. Materials and Methods

2.1. Reagents

NaCl, KCl, Na_2HPO_4 and KH_2PO_4 were used for phosphate buffered saline (PBS 1X) preparation and obtained from Merck. Fetal Bovine Serum (FBS), Dulbecco's Modified Eagle Medium (DMEM), TrypLE express enzyme (1X) with phenol red and 10.0 U/ml penicillin and 10.0 µg/ml streptomycin were purchased by Gibco (Life Technologies). Mammary Epithelial Basal Medium (MEBM) and SingleQuots (hydrocortisone, bovine pituitary extract (BPE), epidermal growth factor human recombined (rhEGF) and recombinant human insulin) were purchased as a MEGM BulletKit™ from Lonza.

Cholera toxin from *Vibrio cholera*, trypsin inhibitor from Glycine max (soybean) and glutaraldehyde solution (50% in water) were from Sigma-Aldrich.

Two different solutions of dimethyl sulfoxide (DMSO) were used: a DMSO from Sigma-Aldrich and a DMSO for UV spectroscopy (≥99.8%) from Merck. The MTT (3-(4,5-dimethylthiazol-2-yl)-2,5-diphenyltetrazolium bromide) tetrazolium solution was prepared using MTT powder from Invitrogen.

2.2. Peptides

pepR was synthesized as C-terminal carboxamides on Rink amide MBHA resin (Novabiochem, Läufelfingen, Switzerland) using standard 9-fluorenylmethyloxycarbonyl (Fmoc) solid-phase synthesis methods in a model 433 automated synthesizer (Applied Biosystems, Foster City, CA) running standard FastMoc protocols at 0.1 mmol scale. Eightfold excess of Fmoc-L-amino acids and HBTU/HOBt, in the presence of double that molar amount of DIEA, was used for the coupling steps, with DMF as solvent. All side-chain functions were protected with TFA labile groups (as described in [29], [30]).

The extraction and purification of PvD1 was carried out in Brazil, as described by O Mello [46], according to the existing collaboration with Universidade Estadual do Norte Fluminense Darcy Ribeiro, Laboratório de Fisiologia e Bioquímica de Microrganismos.

Lyophilized HNP-1 (Bachem) was firstly dissolved in filtered milli-Q water to the final concentration of 1mM and two different pepR solutions were prepared in filtered milli-Q water to the final concentrations of 825.5 and 826.9 µM, respectively. Both peptides, for cell-related studies, were then diluted in sterile PBS buffer (1X, pH 7.4). Two solutions of PvD1 were also prepared in sterile PBS buffer (1X, pH 7.4) to the final concentrations of 400 and 550 µM. Then, for complete dissolution of PvD1, the solution was sonicated for 3 minutes on a transsonic 460/H from Elma (Singen, Germany).

2.3. Biological material

Human breast cell line (MCF 10A) was purchased from ATCC (American Type Culture Collection ATCC® CRL-10317™). These non-tumorigenic cells were obtained from an epithelial tissue derived from a mammary gland of a female patient (36 years old) with fibrocystic disease [82].

Human breast cancer cell line (MDA-MB-231) was also purchased from ATCC and was obtained from an epithelial tissue derived from a metastatic site of mammary gland of a female patient (51 years old) with adenocarcinoma [83].This cell line is described as highly malignant, resistant to chemotherapy drugs and, unlike MCF 10A, grow independently of anchorage or growth factors [84].

2.4. Cell Culture

All this procedure was carried out under aseptic conditions in a laminar flow hood Faster VS-4 (Interlab, Rome, Italy) and cells were maintained in a humidified environment at 37ºC and 5% CO_2 in a CO_2 incubator MCO-18AIC (Sanyo, Japan).

Human breast cancer cell line (MDA-MB-231) was cultured as a monolayer in DMEM medium supplemented with 10% FBS, 10.0 U/ml penicillin and 10.0 µg/ml streptomycin at 37ºC and 5% CO_2. For subculturing, the medium was removed and cells were washed with sterile PBS buffer (1X, pH 7.4). Trypsin was added to the cells and incubated for 3 minutes. When the majority of the cells were detached, supplemented medium was added in order to inhibit trypsin action. The cell suspension was transferred to a sterile tube and centrifuged at 1250rpm and 21ºC for 5 minutes in a centrifuge 5810 R (Eppendorf, Hamburg, Germany). The supernatant was removed and the pellet ressuspended in supplemented medium. The subculturing ratios used for this cell line were 1:5 to 1:50 in new culture vessels, T-25 and T-75 from Thermo Fisher (Roskilde, Denmark). All reagents were preheated to 37ºC in a water bath from Memmert (Schwabach, Germany).

Human breast cell line (MCF 10A) was cultured as a monolayer in MEBM medium supplemented with SingleQuots provided with the Bulletkit, except the GA-1000 (gentamycin-amphotericin B solution). Instead, a 10.0 U/ml penicillin and 10.0 µg/ml streptomycin solution was used. Additionally, to make the complete growth medium, 100ng/ml cholera toxin was added. For subculturing procedure, the medium was removed and cells washed with sterile PBS buffer (1X, pH 7.4). Trypsin was added to cells and incubated for 15 minutes. When the majority of cells were rounded up, trypsin inhibitor from Glycine max (soybean) (Sigma) was added in order to inhibit trypsin action. Cell suspension was transferred to a sterile tube and centrifuged at 1000rpm and 21ºC for 5 minutes. The supernatant was removed and the pellet ressuspended in MEBM medium. The subculturing ratios used for this cell line were 1:3 and 1:4 in new culture vessels, T-25 and T-75.

Both cell lines were observed with an optical microscope, Primovert (Zeiss Germany) and counted with a cell counter (Scepter 2.0 from Milipore).

2.5. Cell viability assay

Human breast cancer cells (MDA-MB-231) and human breast cells (MCF 10A) were counted, diluted to the final concentrations of $3x10^4$ cells/ml and $5x10^5$ cells/ml, respectively, seeded in a 96-well plate and incubated for 24 hours. Thereafter the medium was removed, the peptides solutions were prepared in serum-free medium and added to the wells. For both cell lines, pepR was tested between 0.1 µM and 100 µM and PvD1 was from 0.01 µM to 100 µM, whereas HNP-1's concentrations range from 0.1 µM to 100 µM for MDA-MB-231 and 0.1 µM to 110 µM for MCF 10A. Each concentration was tested at least in triplicate for MDA-MB-231 and in duplicate for MCF 10A, in three different days. All assays had a negative control (100% cell death), 20% DMSO-containing medium for MDA-MB-231 and 30% DMSO-containing medium for MCF 10A, and a positive control (100% viability) with serum-free medium for both cell lines (untreated cells). After 24 hours of incubation 10 µl of 5 mg/ml MTT in PBS buffer (1X, pH 7.4) was added to each well and incubated for 2 hours. Next, the medium with peptide and MTT solution was removed and 150 µl/well of DMSO for UV spectroscopy was added. The absorbance of each well was measured at 540 nm using a microplate reader TECAN infinity F500.

The percentage of viability was calculated as:

$$\%\ Cell\ viability = \frac{Absorbance_{treated\ cells}}{Absorbance_{untreated\ cells}} \times 100 \quad (2)$$

And the percentage of cell death was calculated as:

$$\%\ Cell\ death = 100 - \%\ Cell\ viability \quad (3)$$

The half maximal inhibitory concentration (IC_{50}) values were obtained by fitting the cell death percentage as a function of the logarithm of the inhibitor concentration and are shown as an average of at least three independent experiments. This parameter allows to know the required concentration of an inhibitor which reduces by half the metabolically active cells, is fundamental in pharmacology for comparison of drugs under the same experiment conditions and is describe as a dose-response curve.

2.6. Zeta Potential measurements

Each cell line was detached using trypsin (as described in section 2.4) and then was centrifuged, MDA-MB-231 at 1300rpm and MCF 10A at 1000rpm, both for 5 minutes on a MiniSpin centrifuge (Eppendorf, Hamburg, Germany). The supernatant was removed and the pellet ressuspended in sterile PBS (1X) buffer (pH 7.4).

Human breast cell lines (MDA-MB-231 and MCF 10A) were diluted in sterile PBS buffer (1X) to the final concentration of $1x10^5$ cells/ml and then, different peptide concentrations were added. The cell suspension was transferred to a disposable zeta cell with platinum-gold coated electrodes (DTS1070 from Malvern Instruments, Worcestershire, UK) to the final volume of 800µl and allowed to equilibrate for 30 minutes at 37^0C. A set of 15 measurements (~70 runs each) was performed with a constant voltage of 40 V. The complete experiment was carried out at least 2 times using independent preparations and peptide solutions on a Zetasizer Nano ZS (Malvern Instruments, Worcestershire, UK).

2.7. Atomic Force Microscopy

Human breast cancer cell line (MDA-MB-231) and human breast cell line (MCF 10A) were diluted to the final concentration of $1x10^4$ cells/ml and $1x10^5$ cells/ml, respectively, seeded in a tissue culture dish with 40mm of diameter from TPP (Switzerland) and incubated for 24 hours. After 24 hours the medium was removed and the cell monolayer was washed three times with 1ml of sterile PBS buffer (1X, pH 7.4). For the control images, the culture medium was replaced by serum-free medium and for the assays with PvD1 the culture medium was replaced by serum-free medium with 0.01µM, 0.8µM and 50µM of PvD1.

After 24 hours of incubation, for both cell lines, the medium was removed and the cell monolayer was washed three times with 1ml of sterile PBS buffer (1X, pH 7.4) and three times with 1ml of sterile distilled water. Cell fixation was carried out by adding 1ml of 1% glutaraldehyde in sterile PBS buffer (1X, pH 7.4) for 10 minutes at room temperature. The glutaraldehyde solution was removed and the cell monolayer was washed again three times with 1ml of sterile PBS buffer (1X pH 7.4) and three times with 1ml of sterile distilled water. The dishes were allowed to dry inside the laminar flow hood.

AFM images were acquired using a JPK Nano Wizard II (Berlin, Germany) mounted on a Zeiss Axiovert 200 inverted microscope (Göttingen, Germany). The AFM head is equipped with a 15-µm z-range linearized piezoelectric scanner and an infrared laser. Measurements were carried out in air and in contact mode using uncoated silicon ACL cantilevers from Applied NanoStructure (Santa Clara, CA, USA). ACL cantilevers had typical resonance frequencies between 160 and 225 kHz and an average spring constant of 36-90 N/m. Cells were first visualized through the optical microscope before being selected for imaging. The total scan areas

with 100 × 100 μm were imaged with a resolution of 512 × 512 pixels and scan speeds of 0.2 Hz for MDA-MB-231 and between 0.2 and 0.4Hz for MCF 10A.

The height profiles of cells were acquired drawing a line over each cell with the section tool which opens a cross-section of that region using the JPK SPM Data Processing version 4.2.61. The root-mean-square roughness, R_{ms}, was determined in three different regions (nucleus, cytoplasm and perinuclear area) in five different squared areas (2.5 x 2.5 μm^2) from AFM height images and using Gwyddion 2.24 version software. The AFM image was leveled with a three point level tool and then each square was fitted by a polynomial background tool which stretches the image allowing the entire surface of the cells to become visible. The final R_{ms} value was calculated as the average of all squares analyzed.

2.8. Statistical analysis

The viability and cell death percentages were calculated using Microsoft Office Excel 2010 and the IC_{50} values were computed by GraphPad Prism 5 software.

Zeta-potential, R_{ms}, height profiles and respective standard deviations were processed with GraphPad Prism 5 software. Pairwise significances were calculated using one-way ANOVA followed by a Tukey post-test. The p-values lower than 0.05 were considered significant.

3. Results and Discussion

3.1. Peptides' Cytotoxic Activity

In the last decades, the interest in AMPs has been increased associated with the antibiotic resistance problem. In order to find an alternative to conventional antibiotics, a large number of studies have been carried out using peptides from different sources such as mammalians, insects, plants or even synthesis. With the growing number of studies in the antimicrobial peptides field it was found that some of these AMPs have also a broad spectrum of cytotoxic activity against cancer cells. In this work, three different peptides, known as AMPs, were tested as potential anticancer peptides against human breast cells.

pepR and PvD1 have only proven to be antimicrobial [29] and antifungal peptides [48], respectively, however, some authors have been pointing out to a possible activity as an anticancer peptides [30], [44], [85]. On the other hand, studies with the α-defensin, HNP-1, have shown that, in addition to the innate antimicrobial activity, this peptide also acts as ACP in many different cancer cells [6], [42][42]. However, according with literature, this family of defensins is not tumour selective, causing lysis of healthy cells [6], [35], [86].

In order to evaluate the anticancer activity of each peptide an MTT assay was carried out, where the breast cancer cell line, MDA-MB-231, was exposed to increasing concentrations of each peptide for 24 hours and the IC_{50} value was calculated. Figure 3.1 represents the percentage of cell death resulting from exposure to different peptide concentrations. All three peptides showed cytotoxic activity against cancer cells, as previously proposed, and HNP-1 was once again able to kill cancer cells. It can be concluded that PvD1 is the most efficient ACP at low concentrations, presenting an IC_{50} value of 0.8 ± 1.2 μM, followed by pepR with 2.6 ± 1.1 μM and HNP-1 with 15.2 ± 1.1 μM.

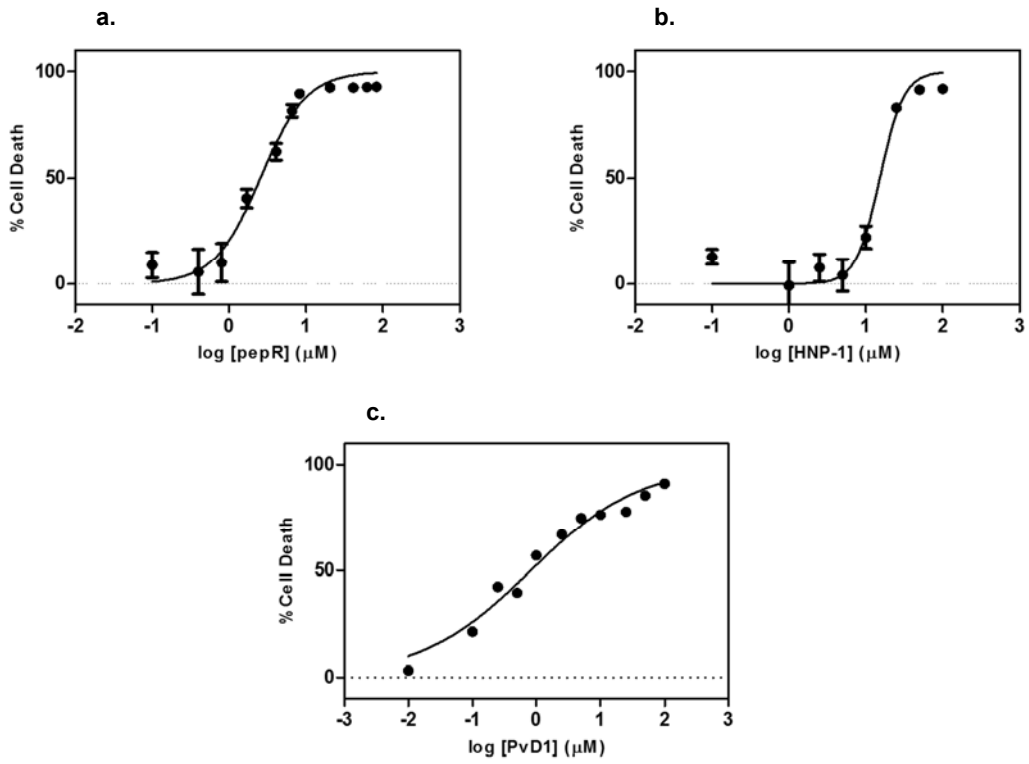

Figure 3.1 – Cytotoxic activity assays of pepR (**a.**), HNP-1 (**b.**) and PvD1 (**c.**) against breast cancer cells (MDA-MB-231). The cytotoxicity of each peptide was assessed 24 hours after peptide's addition using a MTT assay. Error bars represent the standard deviation of at least three independent experiments.

One of the major advantages of AMPs is their ability to be selective. After the anticancer activity of these peptides was confirmed, the same assays were carried out but at this time with a non-tumorigenic breast cell line, MCF 10A, in order to investigate the selectivity of each peptide. As shown in Figure 3.2, all of them also kill non-tumorigenic cells, however, only HNP-1 kills healthy cells with a lower concentration than cancer cells. pepR requires approximately 5 times more concentration to reach the half maximal inhibitory concentration (IC_{50}) and, in case of PvD1, although it was not possible to calculate the IC_{50} value, the reduction by half of the metabolically active cells was reached approximately at 10 μM.

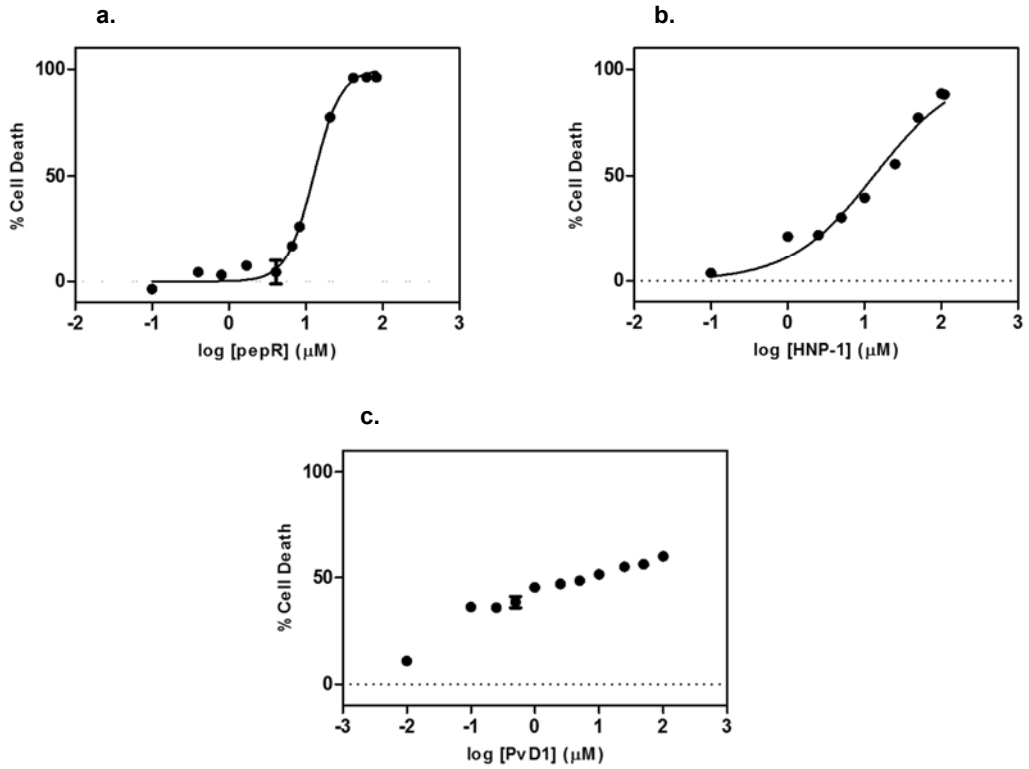

Figure 3.2 - Cytotoxic activity assays of pepR (**a.**), HNP-1 (**b.**) and PvD1 (**c.**) against non-tumorigenic breast cells (MCF 10A). The cytotoxicity of each peptide was assessed 24 hours after peptide's addition using a MTT assay. Error bars represent the standard deviation of at least three independent experiments.

The results obtained for each peptide against both cancer and non-tumorigenic cell lines were then compared in Table 3.1. According with presented IC_{50} values it can be concluded that both pepR and PvD1 are potential ACPs thanks to the low concentration required to kill cancer cells, when compared with the higher concentration required to kill non-tumorigenic ones, being PvD1 the most promising from both. HNP-1, on the other hand, is not able to select between cancer and normal cells, killing both cell lines at the same concentration. Similar results were previously described [35], [42], [86].

Table 3.1 - IC_{50} values and respective standard deviation of each peptide in the presence of breast cancer cells and non-tumorigenic breast cells which are determined from the cytotoxic assays. NA, "not applicable".

	pepR	**HNP-1**	**PvD1**
MDA-MB-231	2.6 ± 1.1 μM	15.2 ± 1.1 μM	0.8 ± 1.2 μM
MCF 10A	12.6 ± 1.1 μM	13.3 ± 1.2 μM	NA

3.2. Characterization of cells' membrane surface charge

Zeta-potential is a light-scattering technique commonly used to study the alterations on membrane surface charge of any particle in solution. This technique was used to study the electrostatic properties of the cell's surface as well as the peptide-cell interactions.

At the first step of zeta-potential analysis, the membrane's surface charge of both cell lines without peptides was measured. For MDA-MB-231, a zeta-potential of -22.99 ± 2.75 mV and the respective electrophoretic mobility of -2.20 ± 0.26 μmcm/Vs was obtained, whereas for MCF 10A, a zeta-potential of -25.0 ± 0.87 mV and a electrophoretic mobility of -2.40 ± 0.09 μmcm/Vs was obtained. Contrary to what would be expected, both cell lines presented a similar negative membrane surface charge.

Zhang et al [87] have already studied the surface charge of MCF7 (breast cancer cells) and MCF 10A which presented a zeta-potential value of -20.32 ± 2.43 mV and -31.16 ± 1.12 mV, respectively. These authors also presented a more negative surface charge value for non-tumorigenic cells and attributes this to the presence of sialic acid anions at the membrane's surface, as well as described by Cook and Jacobson [88].

As previously described, the cancer cells' membrane is constituted by different negative phospholipids which should give a negative charge to the outer leaflet of the membrane. However, according to Papo and Shai [24], these phospholipids correspond to 3-9% of the total membrane phospholipids, giving only a slight negative charge to the cancer cells when compared with the non-tumorigenic ones. Besides phospholipids, the surface of many cells is also composed by glycoconjugates which have ionogenic groups, such as sialic acid (a wide family of related nine-carbon sugar acids), at their terminal position [89]. On the other hand, Cook and Jacobson [88] refer that the presence of these ionogenic groups, mostly sialic acid, at the cells' peripheries are the main responsible for the cells' membranes electrophoretic properties. Thus, it can be speculated that, although the plasma membrane of cancer cells is actually negative compared to healthy cells, due to their phospholipids constitution, there are other components, such as sialic acid, at their surface that confers similar negative charge to both cells when measured by zeta-potential [88].

Some authors have already presented zeta-potential or electrophoretic mobility values from different cells which are in agreement with the negative ones obtained from healthy cells in this work, as can be seen from the Table 3.2.

Table 3.2 – Zeta-potential or electrophoretic mobility values of different healthy and cancer cells according to several authors.

Cells	zeta-potential (mV)	Electrophoretic Mobility (μ/sec./V/cm)	Authors
Normal lymph nodes Leukaemic cells		-1.27 ± 0.03 -1.04 ± 0.04	Cook and Jacobson (1967) [88]
Heathly platelets Leukaemia	-14.2 ± 1.64 -12.81 ± 2.05		Tatsumi et al (1992) [90]
MCF 10A MCF7	-31.16 ± 1.12 -20.32 ± 2.43		Zhang et al (2008) [87]
BCEC HUVEC	-15.28 ± 0.58 -12.89 ± 0.56		Ribeiro et al (2011) [91]
Lung carcinoma	-14.76 ± 1.49		Gaspar et al (2012) [92]
Platelets RBC	-10.75 ± 1.17 -10.80 ± 1.63		Ribeiro et al (2012) [30]
PC-3 MOLT-4	-19.6 ± 1.9 17.8 ± 1.5		Gaspar et al (2014) [42]

According with the results of cytotoxic activity assays it was possible to choose different peptides' concentrations corresponding to below IC_{50}, IC_{50} and above IC_{50}. For pepR two concentrations above the IC_{50} was used whereas for HNP-1 two concentrations below the IC_{50} value were used.

The zeta-potential of breast cancer cells when exposed to each peptide was analysed. As can be seen in Figure 3.3 a., the addition of pepR to the MDA-MB-231 did not induce any significant difference in membrane's surface charge, except far above the IC_{50}. Alves et al [29] has carried out a similar assay with bacteria (*E. coli*) and concluded that cell death is preceded by the complete membrane surface charge neutralization which could indicate that pepR has different modes of action according to its target.

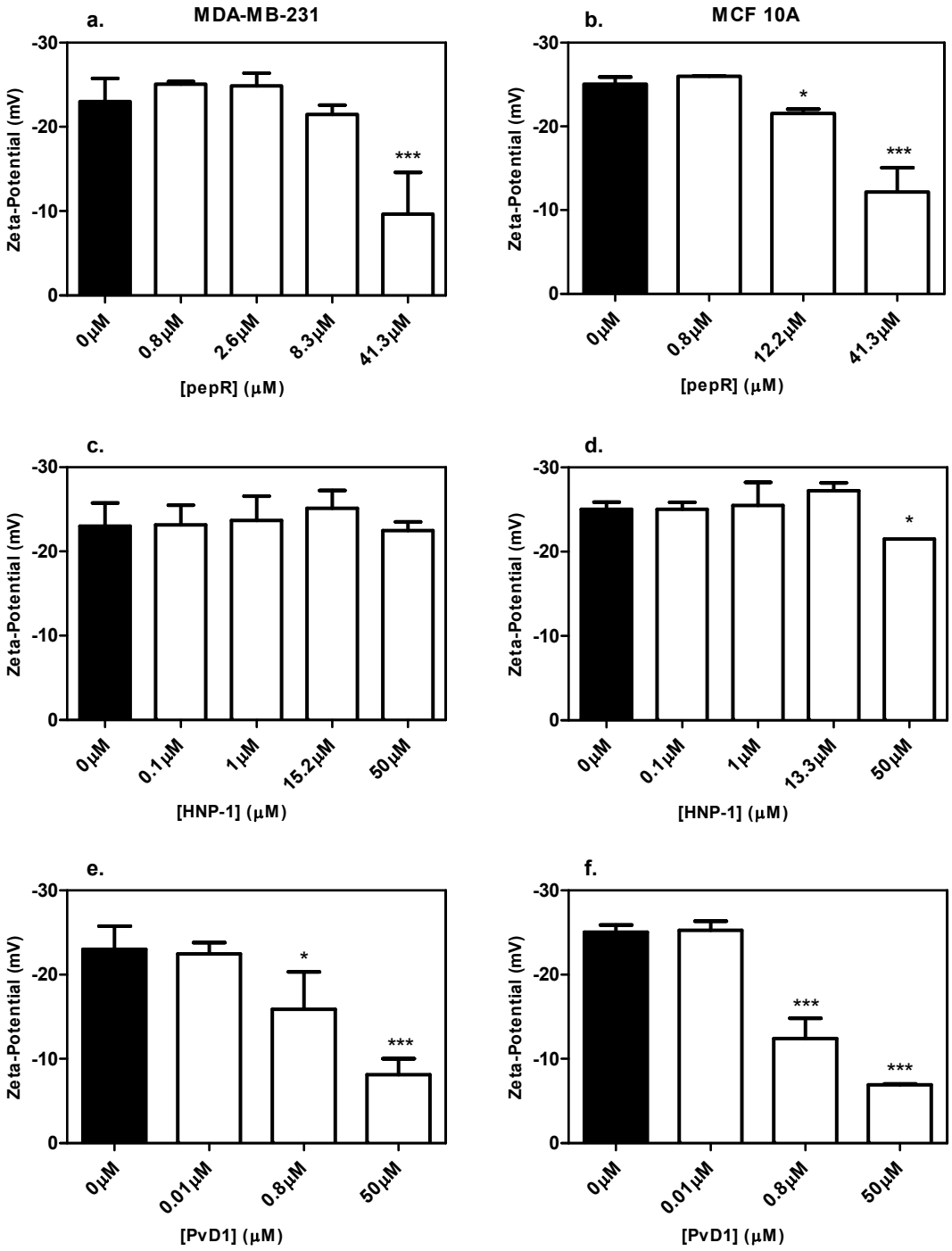

Figure 3.3 – Zeta-potential of MDA-MB-231 (left column **a.**, **c.** and **e.**) and MCF 10A (right column **b.**, **d.** and **f.**) in the presence of pepR (**a.** and **b.**), HNP-1 (**c.** and **d.**) and PvD1 (**e.** and **f.**). Cell suspension of $1x10^5$cells/ml was stabilized for 30 minutes with different concentrations of peptide and the zeta-potential was measured at 37ºC. Error bars represent the standard deviation of at least two independent experiments. As statistical analysis a one-way ANOVA followed by a Tukey post-test was used. * 0.01 < p-value < 0.05; *** p-value < 0.0001.

HNP-1 was also added to a breast cancer cells suspension in an increasing range of concentrations (Figure 3.3 c.) and did not induce any significant difference in membrane surface charge, not even at high peptide concentrations.

The last peptide being tested against cancer cells was PvD1 (Figure 3.3 e.). With the addition of increasing concentrations of PvD1 it was found that this peptide induced a significant increase in membrane surface charge, although, once again, does not lead to complete charge neutralization.

All these essays were repeated for MCF 10A cells, for each peptide, under the same conditions and according with concentrations obtained by the cytotoxic activity assays. Contrary to what was found with cancer cells, pepR starts to induce the increase of membrane surface charge at the IC_{50} value, but once again the total neutralization of the outer leaflet does not precedes the peptide's effect (Figure 3.3 b.).

In Figure 3.3 d. HNP-1 was added to MCF 10A cells and only above the IC_{50} value is a significant increase in membrane surface charge.

Once it was not possible to fit the IC_{50} curve for the PvD1 with MCF 10A, the zeta-potential assays were carried out with the same peptide's concentration used for MDA-MB-231 (Figure 3.3 f.).

According to Figure 3.3 e. and f., PvD1 showed similar behaviour in both cell lines with the only difference being the increase of the MCF 10A surface charge at the IC_{50} which, once again, showed that the mechanism of action of this peptide is not dependent of a previous charge neutralization.

Overall, and contrary to what has been described for these peptides, when they act as AMPs, the anticancer activity is not characterized by the collapse of the membrane's potential (HNP-1) [6], [43], or by full neutralization of membrane's surface (pepR) [29] before cell death occurs. These differences may indicate that the same peptide has different mechanisms of action depending on its target. HNP-1's behaviour as ACP is in agreement with literature [42], since it is not able to select between cancer and healthy cells.

According to Shahidullah and London [93], the cell-peptide interaction depends not only on the membrane charge but also on the peptide's positive charge, showing that this effect increases with the number of positive charges on the peptide. Thus, HNP-1 with a positive charge of +3 showed less effectiveness against MDA-MB-231 when compared with pepR with a positive charge of +12 once the first one needs more peptide to induce cell death and changes at the membrane surface.

3.3. AFM imaging of human breast cells

The AFM is a scanning probe microscopy that allows 3D mapping of a sample surface at the nanoscale [71], [72]. With this technique it is not only possible to study the effect of the anticancer peptide on the surface of the cell membrane as well as access to what happens inside the cells through the surface's mapping.

According to data previously discussed, it has become possible to choose the best among the three different anticancer peptides. Both, pepR and PvD1, proved potential anticancer activity, but PvD1 presented a lower IC_{50} value against cancer cells, which minimizes the amount of peptide required, and, at the same time, proved to be less effective with non-tumorigenic cells at the range of concentrations tested.

Both breast cell lines, MDA-MB-231 and MCF 10A, were once again submitted to PvD1's action, this time, in order to imaging the peptide-cell interaction. Figure 3.4 shows AFM error images of both cell lines in absence of PvD1 and Figure 3.5 and Figure 3.6 show images from the 24 hours incubation of MDA-MD-231 and MCF 10A respectively, with PvD1 at the following concentrations: 0.01 µM, 0.8 µM and 50 µM, as well as in absence of peptide (control).

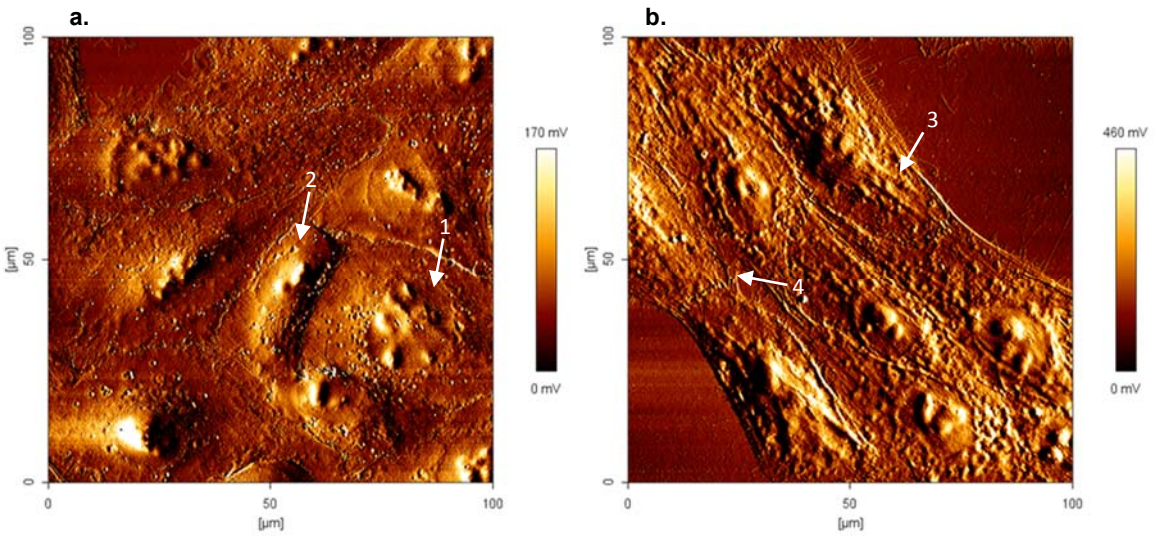

Figure 3.4 – Atomic force microscopy error images (100 x 100 µm) of MDA-MB-231 (**a.**) (1x10^{4}cells/ml) and MCF 10A cells (**b.**) (1x10^{5}cells/ml) (100 x 100 µm), and respective colour scales at right, in absence of PvD1. **1** and **2** indicate a round and pointy shape nucleus of cancer cells, respectively. **3** indicate some structures present in cytoplasm through the membrane and **4** the formation of pseudopodia.

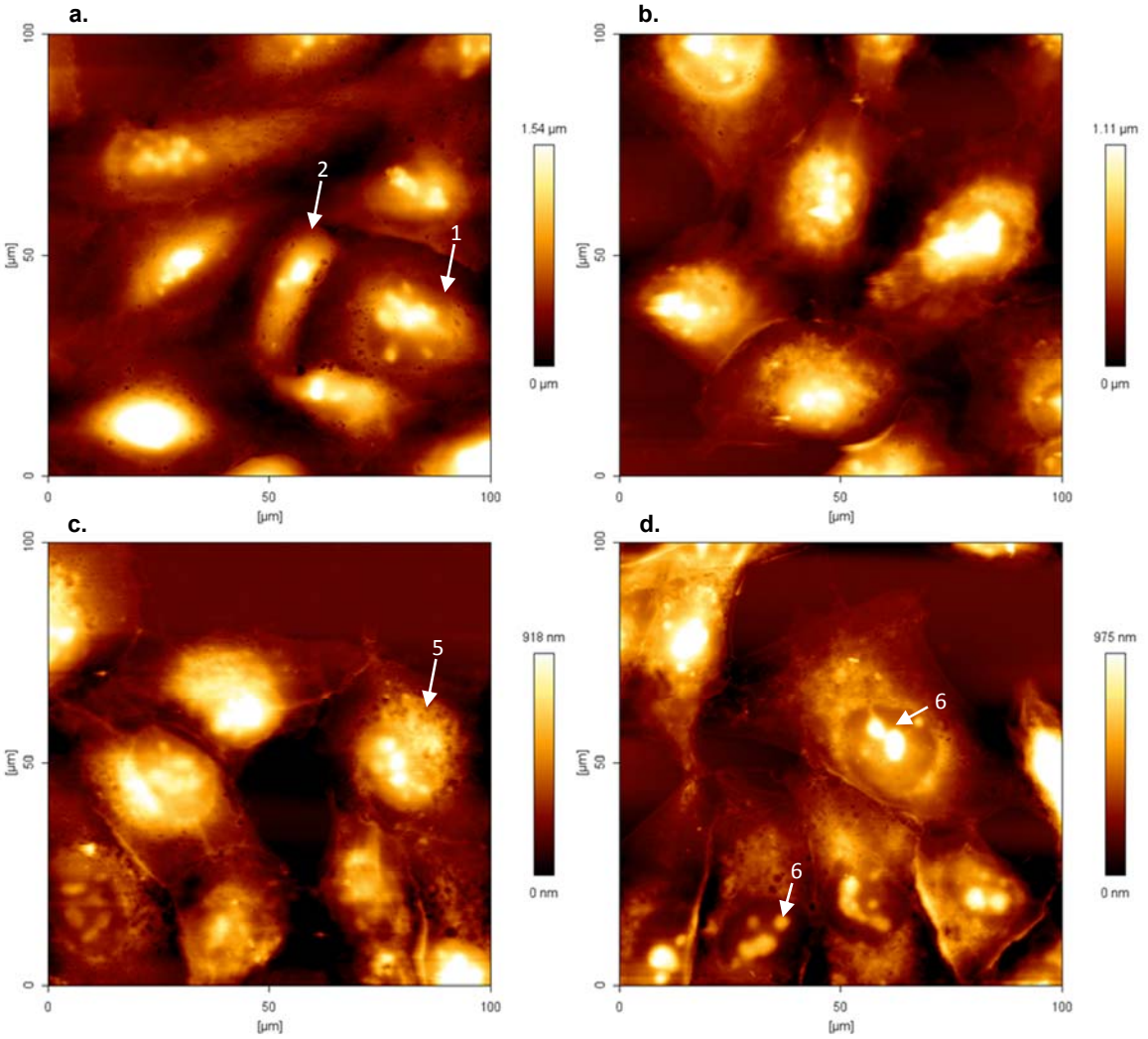

Figure 3.5 – Atomic force microscopy height images of MDA-MB-231 cells (1x10^{4}cells/ml) (100 x 100 µm), and respective colour scales at right, in absence (**a.**) and presence of different concentrations of PvD1, (**b.**) 0.01 µM, (**c.**) 0.8 µM and (**d.**) 50 µM after 24 hours of incubation. **1** and **2** indicate a round and pointy shape nucleus of cancer cells, respectively. **5** indicate the increasing of roughness in the perinuclear region and **6** the nucleoli inside the nucleus.

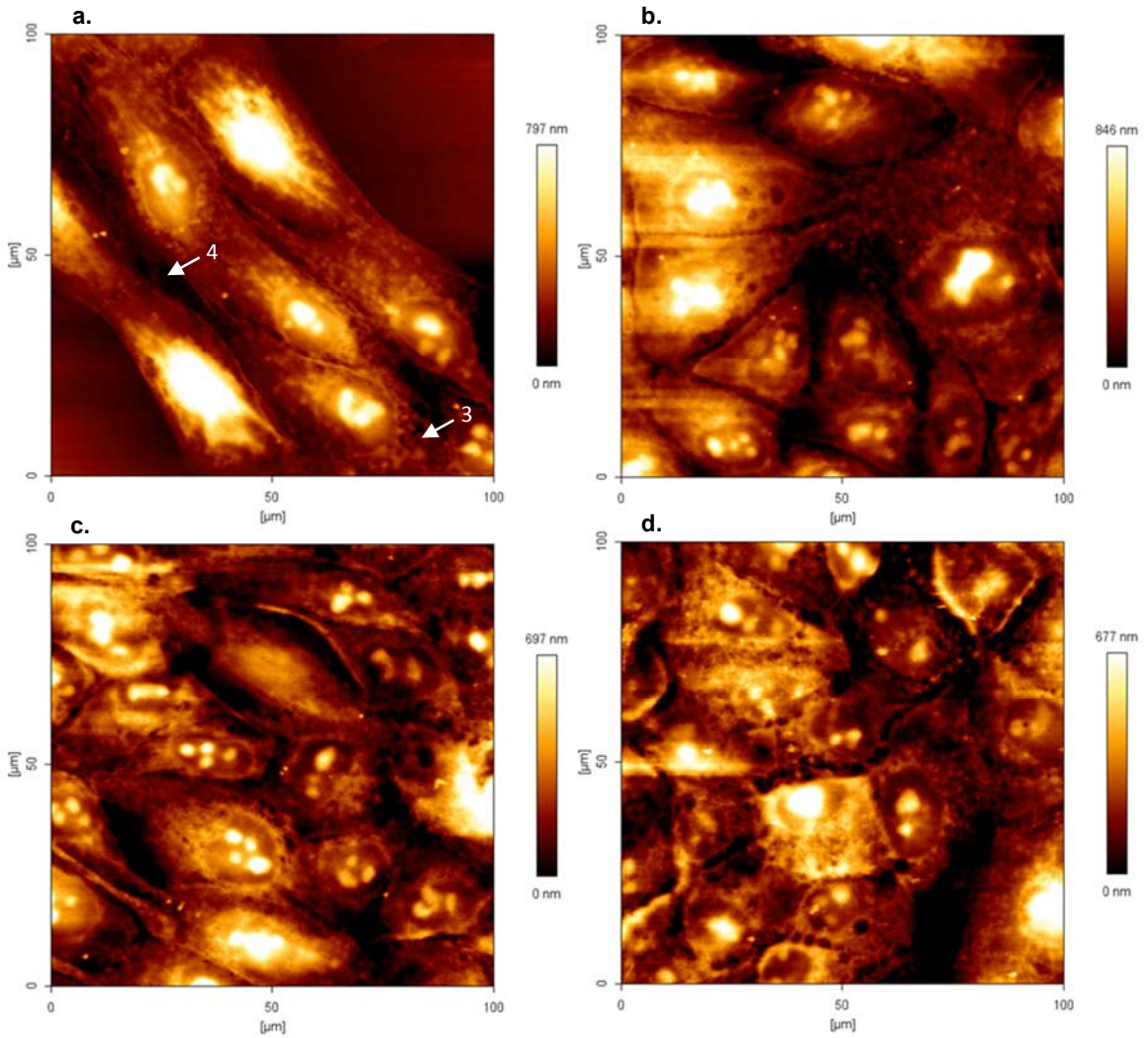

Figure 3.6 - Atomic force microscopy height images of MCF 10A cells (1x10^{5}cells/ml) (100 x 100 µm), and respective colour scales at right, in absence (**a.**) and presence of different concentrations of PvD1, (**b.**) 0.01 µM, (**c.**) 0.8 µM and (**d.**) 50 µM after 24 hours of incubation. **3** indicate some structures present in cytoplasm through the membrane and **4** the formation of pseudopodia.

From the control images obtained by AFM error images, as well as from AFM height images corresponding as a. in Figure 3.5 and Figure 3.6, the morphological differences between both breast cell lines can be seen. The AFM error images of control cells were presented in order to contribute to facilitate the morphological analysis. Both cell lines derived from breast epithelial tissue, however, MCF 10A (Figure 3.4 b. and Figure 3.6 a.) presented as a more organized layer with an elongated shape, when compared with MDA-MB-231 (Figure 3.4 a. and Figure 3.5 a.), due to the alterations induced by transformation process into cancer cells. MDA-MB-231 also showed a high disorder in nuclear morphology presenting very different architectures and sizes [84]. As can be seen in Figure 3.5 a., cancer cells nucleus can acquire a round (1) or pointy (2) shape. MDA-MB-231 also depict a bigger nucleus when compared with the whole cell size. On the other hand, MCF 10A have a more flattened shape than MDA-MB-231 which allows to see some structures present in cytoplasm through the membrane (as 3 in Figure 3.6 a.), especially in the region surrounding the nucleus, namely, perinuclear region. Additionally, it can also be seen

in both cell lines some pseudopodia at the cell's surface (as 4 in Figure 3.6 a.) which is responsible for processes such as cell migration and invasion [94].

With the PvD1 incubation, some surface changes became progressively visible. For both cell lines, when 0.01 μM was added, no changes are visible at the membrane surface cells which are in agreement with previous results, once this concentration is under the IC_{50} value. In MDA-MB-231, after adding 0.8 μM of PvD1, some surface changes became visible, specifically the increasing of roughness in the perinuclear region (as 5 in Figure 3.5 c.), which could indicate that PvD1 acts as ACP in a specific region of the cells. MCF 10A remains with the same appearance showing no changes caused by the presence of PvD1 at 0.8 μM and consequently proving the peptide's selectivity to non-tumorigenic cells. Finally, 50 μM of PvD1 was added to both cell lines and, in case of MCF 10A, an increasing of destruction in perinuclear region of the cells can be seen, making it difficult, in some cells, to distinguish the different cellular regions. MDA-MB-231 shows a decreasing in nucleus height (according with the colour scale) showing the nucleoli present therein (as 6 in Figure 3.5 d.) possibly caused by output of part of the cell content.

3.4. PvD1 effects on cell's height

Following the cells' morphological analysis, height profiles were acquired for each cell drawing a line with the section tool of JPK SPM Data Processing, as described in section 2.7. For MDA-MB-231 45 cells as control, 22 cells for 0.01 μM, 33 cells for 0.8 μM and 23 cells for 50 μM of PvD1 were analysed. For MCF 10A 28 cells as control, 45 cells for 0.01 μM, 41 cells for 0.8 μM and 25 cells for 50 μM were analysed. The cells' highest point is commonly the nucleus region with respectively nucleolus and consequently, the section was always drawn through this cell's region. Figure 3.7 represents the height profiles acquisition. The cells' height average at each PvD1 concentration is organized in Table 3.3 presented for each breast cell line (Figure 3.8). Comparing the obtained height profiles for MDA-MB-231 and MCF 10A without peptide, it could be inferred that breast cancer cells are almost twice higher than non-tumorigenic breast cells, which once again is consistent with the literature [84].

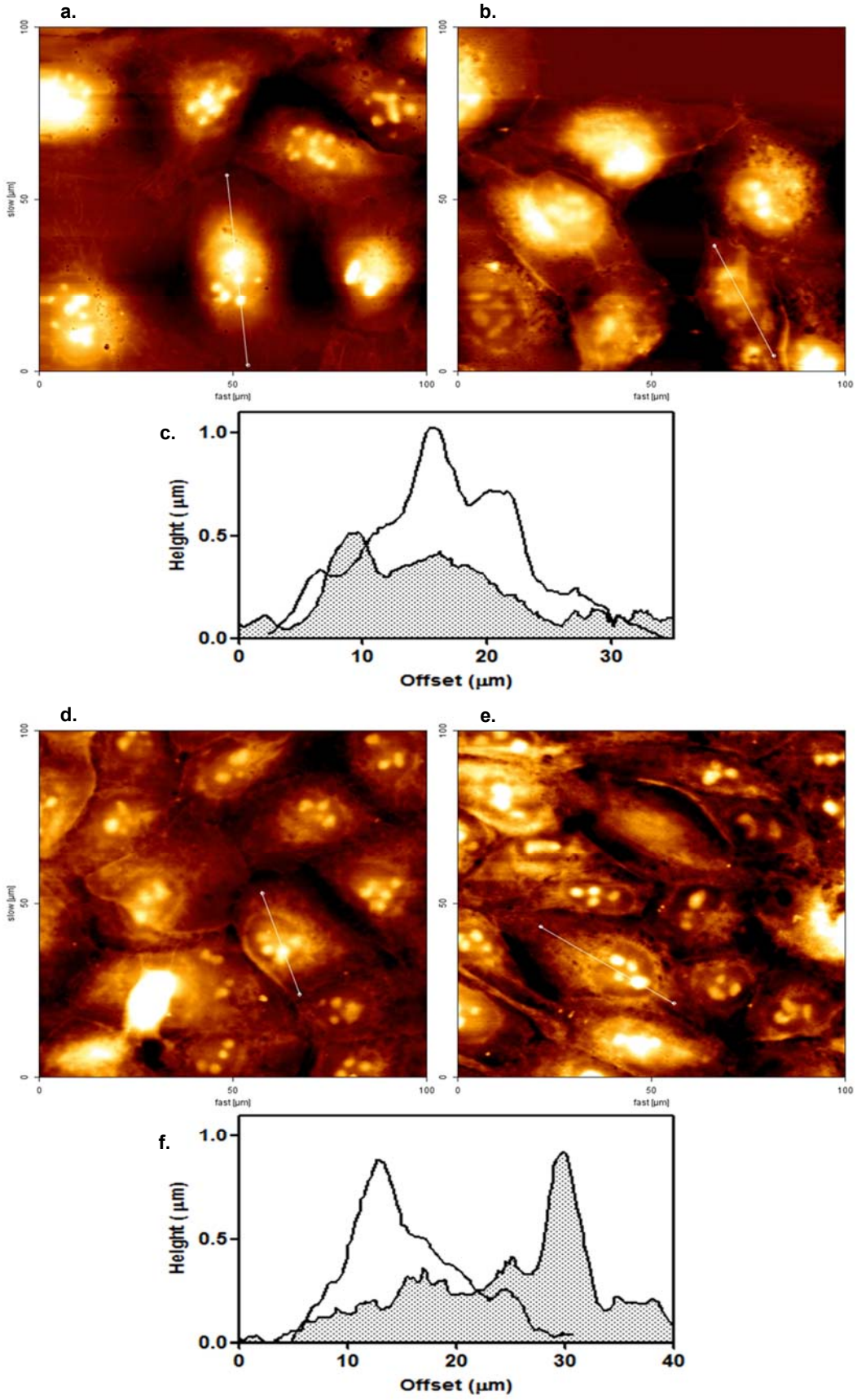

Figure 3.7 – Representative cell's cross sections and height profiles. MDA-MB-231 in absence (a.) and presence (b.) of 0.8 µM of PvD1 with the respective acquired height profile for both cells (c.) in absence (white) and presence (grey) of PvD1. MCF 10A in absence (d.) and presence (e.) of 0.8 µM of PvD1 and respective height profile for both cells (f.) represented with the same colours.

Table 3.3 – Average of cells height and respective standard deviation after incubation with PvD1 peptide.

	Control	0.01 µM	0.8 µM	50 µM
MDA-MB-231	1.3 ± 0.4 µm	1.2 ± 0.2 µm	1.0 ± 0.3 µm	1.1 ± 0.4 µm
MCF 10A	0.7 ± 0.2 µm	0.7 ± 0.2 µm	0.6 ± 0.2 µm	0.5 ± 0.2 µm

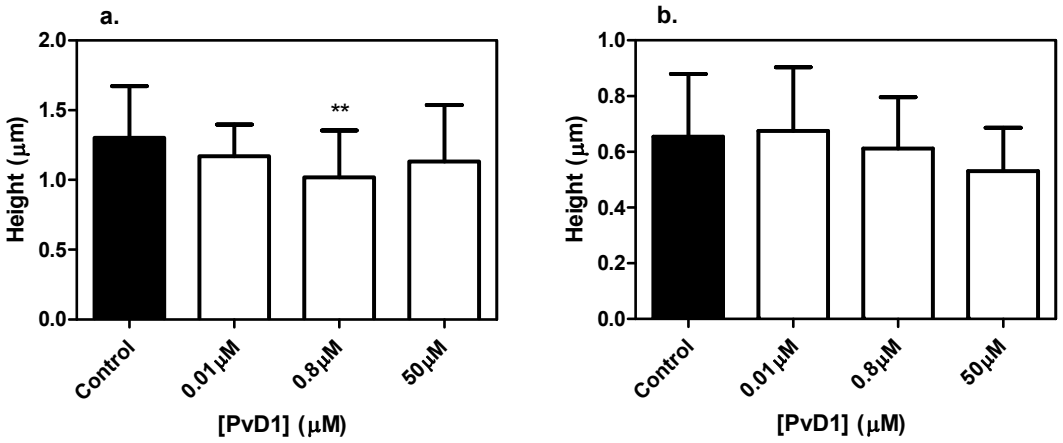

Figure 3.8 – MDA-MB-231 (**a.**) and MCF 10A (**b.**) cell's height in absence and presence of different concentrations of PvD1. Error bars represent the standard deviation of at least two independent experiments. As statistical analysis a one-way ANOVA followed by a Tukey post-test was used. ** 0.0001 < p-value < 0.01.

Contrary to what would be expected, according to AFM images, (Figure 3.5 and Figure 3.6) after the incubation with PvD1 only slight variations in cells' height occur and in the case of MCF 10A no statistical significance was found. It is not possible to propose a cell death mechanism induced by the increasing of PvD1 concentration since it is not visible cell swelling or apoptotic bodies. However, the reduction of height in MDA-MB-231 can be characteristic of an apoptotic process.

3.5. Surface roughness as indicator of cell's homeostasis

Surface roughness is a widely used parameter to evaluate the homeostasis of cells, once it is involved in different mechanisms such as intracellular contact, motility, adhesion and a good indicator of membrane-skeleton structure [42], [95], [96]. To better understand the effects of PvD1 in cells' membrane, surface roughness of different cells' regions were analysed. For each cell, and using Gwyddion software, the R_{ms} value was obtained in five different squares of 2.5 x 2.5

μm^2 from three different regions: nucleus, cytoplasm and perinuclear region. Once again for MDA-MB-231 45 cells as control, 22 cells for 0.01 μM, 33 cells for 0.8 μM and 23 cells for 50 μM of PvD1 were analysed and for MCF 10A 28 cells as control, 45 cells for 0.01 μM, 41 cells for 0.8 μM and 25 cells for 50 μM were analysed. The average roughness of each cell region according to the PvD1 concentration is presented in Table 3.4 and Figure 3.9. Additionally, it was also calculated the average roughness of the whole cells, represented in Figure 3.10 and Table 3.5.

Table 3.4 – Average of surface root-mean-square roughness (R_{ms}) of MDA-MB-231 and MCF 10A cells in absence and presence of different PvD1 concentrations.

		MDA-MB-231	**MCF 10A**
PvD1 (μM)	**Cell region**	**R_{ms} (nm) ± SD**	**R_{ms} (nm) ± SD**
Control	Cytoplasm	18.5 ± 8.8	21.5 ± 7.4
	Nucleus	52.6 ± 25.7	48.6 ± 20.0
	Perinuclear	51.0 ± 18.3	33.4 ± 15.6
0.01 μM	Cytoplasm	23.6 ± 16.1	20.4 ± 5.0
	Nucleus	48.4 ± 28.5	39.6 ± 12.6
	Perinuclear	46.8 ± 26.8	29.9 ± 7.5
0.8 μM	Cytoplasm	27.3 ± 11.6	22.6 ± 6.3
	Nucleus	43.4 ± 18.0	35.7 ± 15.6
	Perinuclear	44.6 ± 21.2	29.0 ± 7.0
50 μM	Cytoplasm	41.4 ± 14.0	32.6 ± 11.9
	Nucleus	53.3 ± 34.7	33.0 ± 10.9
	Perinuclear	51.7 ± 20.6	37.2 ± 14.4

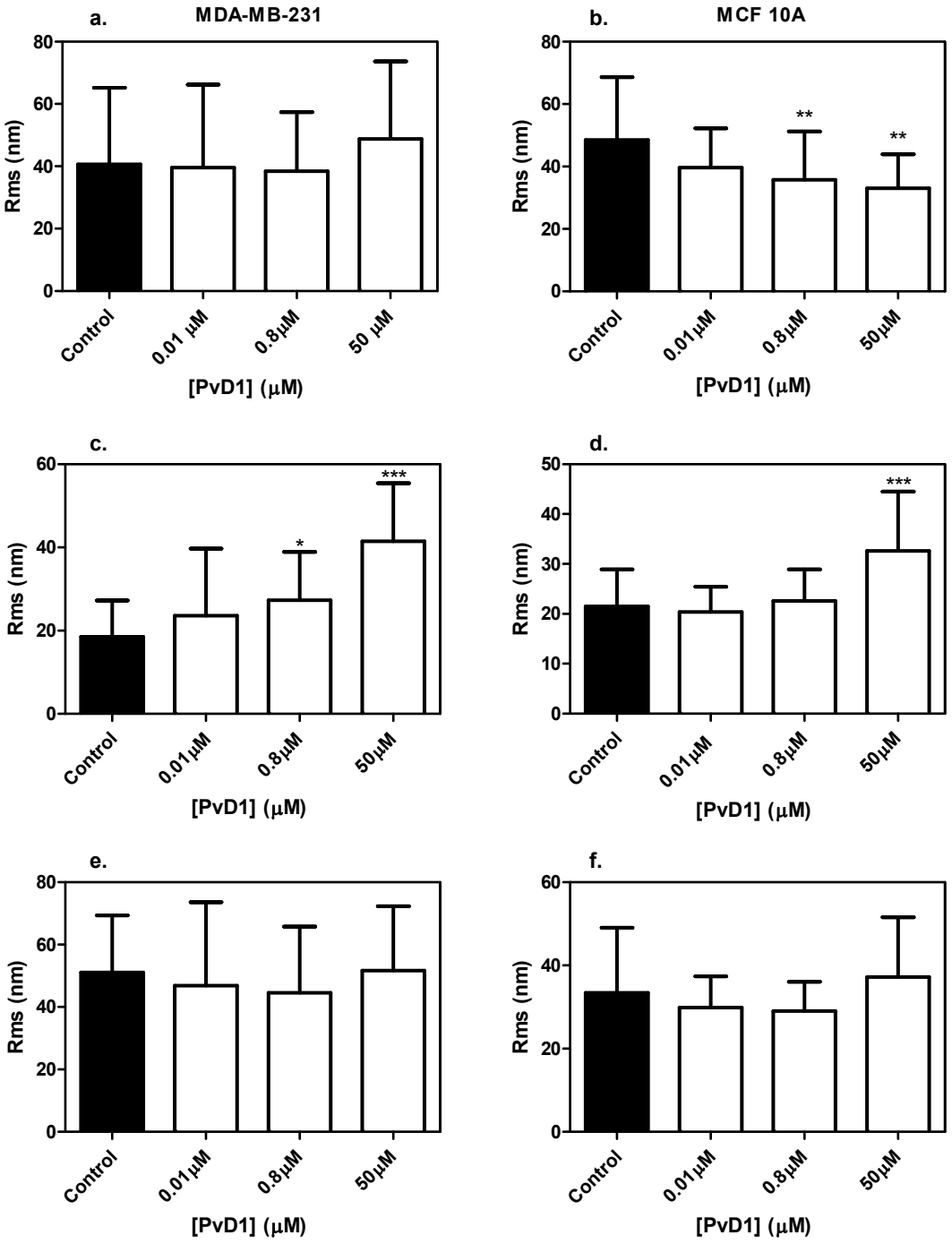

Figure 3.9 - Surface root-mean-square roughness (R_{ms}) average of MDA-MB-231 (left column **a.**, **c.** and **e.**) and MCF 10A cells (right column **b.**, **d.** and **f.**) in different cell regions: nucleus (**a.** and **b.**), cytoplasm (**c.** and **d.**) and perinuclear region (**e.** and **f.**), respectively. The average roughness of each cell region was obtained as the average of five different squares of 2.5 x 2.5 μm^2. Error bars represent the standard deviation of at least two independent experiments. As statistical analysis a one-way ANOVA followed by a Tukey post-test was used. ** 0.0001 < p-value < 0.01; *** p-value < 0.0001.

According to the data depicted in Figure 3.10, and unlike what would be expected, the R_{ms} value of cells as a whole indicates that PvD1 does not induced statistically significant changes

on cells' surface roughness. Only when analysing each region independently (as seen in Figure 3.9) the changes induced by the peptide became noticeable. Namely, at cytoplasm level, both cell lines present an increasing in surface roughness whereas in MCF 10A a decrease of surface roughness arise in the nucleus.

Table 3.5 - Average of surface root-mean-square roughness (R_{ms}) of MDA-MB-231 and MCF 10A cells as a whole in absence and presence of different PvD1's concentrations.

	Control	0.01 µM	0.8 µM	50 µM
MDA-MB-231	40.7 ± 24.5 nm	39.6 ± 26.6 nm	38.4 ±19.0 nm	48.8 ± 24.9 nm
MCF 10A	34.5 ± 18.8 nm	30.0 ± 11.9 nm	29.1 ± 11.7 nm	34.3 ± 12.5 nm

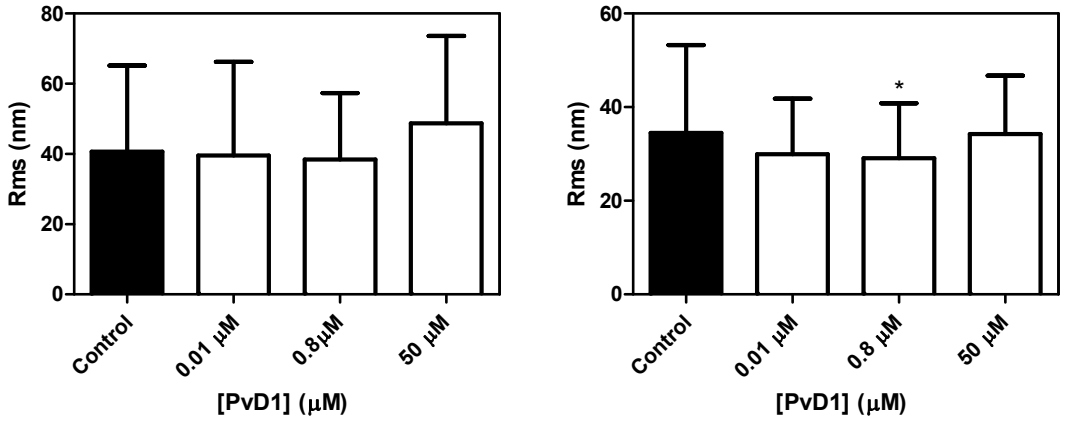

Figure 3.10 - Surface root-mean-square roughness (R_{ms}) average of MDA-MB-231 (left) and MCF 10A (right) as a whole cells. The R_{ms} value was obtained as the average of all 2.5 x 2.5 μm^2 squares analysed (from nucleus, cytoplasm and perinuclear region). Error bars represent the standard deviation of at least two independent experiments. As statistical analysis a one-way ANOVA followed by a Tukey post-test was used. * 0.01 < p-value < 0.05.

For the breast cancer cells' interaction with PvD1 at different concentrations, it could be concluded that PvD1 preferably operates in a specific region of MDA-MB-231 once changes induced by peptide's action are only measurable in the cytoplasm region. In that case, it is described as an increased roughness in membrane's surface which is proportional to the PvD1 concentration and is in agreement with the cytotoxic activity assays previously carried out. This result can suggest changes to the structures of cell's membrane, more precisely at the level of lipoproteins, such as been referred by Capozzi [95] and Ghanekar [97].

On the other hand, in MCF 10A, the membrane's surface roughness changes are significant in two different regions of the cells (nucleus and cytoplasm) and mainly at 50 µM of

PvD1. In this case, peptide's interaction induced the decreasing of nucleus roughness together with the increase in concentration of PvD1. As previously described [42], [96], this decreasing in surface roughness may be due to the decreasing in mechanical support exerted by the membrane skeleton on the lipid bilayer. The same cell line, only when was exposed to a high concentration of PvD1 (above the IC_{50} value), presented a pronounced roughness increase at cytoplasm region which could be described, once again, as modifications in lipoproteins of cells' membrane. In fact, as previously referred, with the increasing of peptide concentration the surface changes became visible in AFM images, mainly in the cytoplasm region, showing that the cytoplasm's roughness changes are in agreement with cytotoxic viability assays previously described.

Overall, all peptides tested are already known as potential AMPs [29], [35], [48], but pepR and PvD1 proved to be promising ACPs since both peptides presented some selectivity between cancer and healthy breast cells and preference for the first ones. HNP-1 was confirmed not having selectivity, however, according with previous results, showed a different mode of action in presence of human cells which does not induce a collapse of membrane potential and loss of membrane integrity [6], [43]. Additionally, pepR showed a different mode of action when exposed to human cells, as seen with zeta-potential results, since it does not require the total neutralization of the membrane surface charge before the cell death, as described for *E. coli* [29].

4. Conclusions and Perspectives

Although many efforts have been made in therapy, cancer still remains one of the major causes of death worldwide. There are different treatments such as surgery or radiation, but in the case of advanced or metastatic disease chemotherapy is the most common used. Despite its frequent use, chemotherapy is often associated with side-effects such myelosuppression, mucositis and alopecia due to healthy cell's damage, consequence of a low selectivity and to cancer cells' resistance to treatment [9]. In order to improve the selectivity and efficacy of currently cancer therapies some advances have been made to develope a new class of anticancer drugs.

The growing search for a new class of antimicrobial drugs leads to an increasing in AMPs' research and consequently the discovery of anticancer activity in some AMPs, which can be used as new applications in cancer therapy. In this work three peptides (pepR, HNP-1 and PvD1), known as antimicrobials with different origins (synthesis, human and plants, respectively) were tested as possible ACPs against human breast cancer cells.

In the first phase of the present work the cytotoxic activity of each peptide was tested against breast cancer cells (MDA-MB-231) in order to evaluate their anticancer ability. All peptides, even though at different concentrations, proved to be ACPs, killing cancer cells at low concentrations. But, as previously described, one of the most needed improvements in anticancer drugs is their selectivity to cancer cells. Thus, the same assays were carried out this time with non-tumorigenic breast cells (MCF 10A) for comparison. According to these results both pepR and PvD1 proved to be more efficient killing cancer cells than non-tumorigenic ones. For pepR, five times more concentration is required to induce the same effect on MCF 10A, when compared with MDA-MB-231. For PvD1, it has not been possible to obtain the IC_{50} value for the non-tumorigenic cells, nevertheless, it can be concluded that this peptide is selective. HNP-1, on the other hand, is not able to distinguish between cancer and healthy cells.

In the second part of this work, the surface charge membrane of both cell lines in the presence and absence of each peptides was studied. Despite the difference in membrane's constitution, both cell lines in suspension showed similar zeta-potential values in absence of peptides (MDA-MB-231: -22.99 ± 2.75 mV and MCF 10A: -25.0 ± 0.87 mV). This fact seems to be due to sialic acid which is present in the terminal position of the glycoconjugates at the surface of cells membrane, confers a negative charge to both cells and is known as the main responsible for the cells' electrophoretic properties.

Unlike what was described for antimicrobial activity, when pepR acts as ACP the total membrane surface charge neutralization before cell death is not required. Also HNP-1 showed a different mode of action relative to antimicrobial activity because the collapse of the membrane potential does not occur. However, with PvD1, the increasing of membrane surface charge proved to be concomitant with the concentration and similar for both breast cell lines.

With those results, it could be concluded that PvD1 seems to be the best of the three tested peptides with the lowest IC_{50} value and the biggest difference of action between both cell lines in cytotoxicity assays. In addition, this peptide also showed the biggest difference in surface charge membrane (for both cell lines).

According with the previous conclusions, in the last part of this work, AFM images of PvD1 interaction with both cell lines were obtained and cell's height and surface roughness evaluated for each case. Although PvD1 actually acts as ACP, its effect was not significantly visible in the height profiles or in the surface roughness not allowing draw conclusions about the mechanism of death induced by this peptide. However, according with the reduction of height in MDA-MB-231, when exposed to an increasing concentration of PvD1, an apoptotic process could be proposed.

As future work, also pepR and HNP-1 should be used in atomic force microscopy studies in order to completely evaluate their anticancer ability and peptide-cell interaction. Additionally, the surface area of both breast cell lines should be studied in order to evaluate the effects induced by the absence and presence of different concentrations of peptides. Further studies to the complete PvD1's characterization also should be done.

Future studies as flow cytometry can be carried out in order to better understand the effects of different concentrations of peptides in some aspects such as membrane permeabilization, granularity, cell damage or even cell death progression. This technique will help to evaluate the cell death mechanism induced by each peptide.

Cationic peptides are partially neutralized by anionic components of serum [9], which could indicate a problem in anticancer therapy when using peptides. In that sense, some assays using liposomes as passive delivery of ACPs can be carried out in order to avoid neutralization and simultaneously take advantage of the increased local tissue peptide's concentration.

Subsequently, some *in-vivo* assays (with animal models) must be done for testing the ability of each peptide to act on a living organism and to extrapolate these results in order to be used in humans as ACPs.

5. References

[1] "World Health Organization," *Cancer - Key facts*, 2015. [Online]. Available: http://www.who.int/mediacentre/factsheets/fs297/en/. [Accessed: 15-May-2015].

[2] E. G. Rodrigues, A. S. Dobroff, C. P. Taborda, and L. R. Travassos, "Antifungal and antitumor models of bioactive protective peptides," *An. Acad. Bras. Cienc.*, vol. 81, no. 3, pp. 503–520, 2009.

[3] A. Jemal, F. Bray, M. M. Center, J. Ferlay, E. Ward, and D. Forman, "Global cancer statistics.," *CA. Cancer J. Clin.*, vol. 61, no. 2, pp. 69–90, 2011.

[4] D. Gaspar, A. Salomé Veiga, and M. A. R. B. Castanho, "From antimicrobial to anticancer peptides. A review," *Front. Microbiol.*, vol. 4, 2013.

[5] J. Thundimadathil, "Cancer Treatment Using Peptides: Current Therapies and Future Prospects," *J. Amino Acids*, vol. 2012, pp. 1–13, 2012.

[6] D. W. Hoskin and A. Ramamoorthy, "Studies on anticancer activities of antimicrobial peptides," *Biochim. Biophys. Acta*, vol. 1778, pp. 357–375, 2008.

[7] W. Huang, J. Seo, S. B. Willingham, A. M. Czyzewski, M. L. Gonzalgo, I. L. Weissman, and A. E. Barron, "Learning from host-defense peptides: Cationic, amphipathic peptoids with potent anticancer activity," *PLoS One*, vol. 9, no. 2, 2014.

[8] Y. B. Huang, L. Y. He, H. Y. Jiang, and Y. X. Chen, "Role of helicity on the anticancer mechanism of action of cationic-helical peptides," *Int. J. Mol. Sci.*, vol. 13, pp. 6849–6862, 2012.

[9] S. Riedl, D. Zweytick, and K. Lohner, "Membrane-active host defense peptides - Challenges and perspectives for the development of novel anticancer drugs," *Chem. Phys. Lipids*, vol. 164, pp. 766–781, 2011.

[10] J. B. McPhee and R. E. W. Hancock, "Function and therapeutic potential of host defense peptides," *J. Pept. Sci.*, vol. 11, pp. 677–687, 2005.

[11] G. Wang, B. Mishra, K. Lau, T. Lushnikova, R. Golla, and X. Wang, "Antimicrobial Peptides in 2014," *Pharmaceuticals*, vol. 8, pp. 123–150, 2015.

[12] W. C. Wimley and K. Hristova, "Antimicrobial Peptides: successes, challenges and unanswered questions," *J. Membr Biol*, vol. 239, pp. 27–34, 2011.

[13] Y. Li, Q. Xiang, Q. Zhang, Y. Huang, and Z. Su, “Overview on the recent study of antimicrobial peptides: Origins, functions, relative mechanisms and application,” *Peptides*, vol. 37, pp. 207–215, 2012.

[14] S. T. Henriques, M. N. Melo, and M. A. R. B. Castanho, “Cell-penetrating peptides and antimicrobial peptides: how different are they?,” *Biochem. J.*, vol. 399, 2006.

[15] C. L. Friedrich, D. Moyles, T. J. Beveridge, and R. E. Hancock, “Antibacterial action of structurally diverse cationic peptides on gram-positive bacteria.,” *Antimicrob. Agents Chemother.*, vol. 44, no. 8, pp. 2086–2092, 2000.

[16] E. Badosa, R. Ferre, M. Planas, L. Feliu, E. Besalú, J. Cabrefiga, E. Bardají, and E. Montesinos, “A library of linear undecapeptides with bactericidal activity against phytopathogenic bacteria,” *Peptides*, vol. 28, pp. 2276–2285, 2007.

[17] A. Bonucci, E. Balducci, S. Pistolesi, and R. Pogni, “The defensin-lipid interaction: Insights on the binding states of the human antimicrobial peptide HNP-1 to model bacterial membranes,” *Biochim. Biophys. Acta - Biomembr.*, vol. 1828, pp. 758–764, 2013.

[18] M. Zasloff, “Antimicrobial peptides of multicellular organisms.,” *Nature*, vol. 415, pp. 389–395, 2002.

[19] M.-D. Seo, H.-S. Won, J.-H. Kim, T. Mishig-Ochir, and B.-J. Lee, “Antimicrobial Peptides for Therapeutic Applications: A Review,” *Molecules*, vol. 17, pp. 12276–12286, 2012.

[20] R. E. W. Hancock and H.-G. Sahl, “Antimicrobial and host-defense peptides as new anti-infective therapeutic strategies.,” *Nat. Biotechnol.*, vol. 24, no. 12, pp. 1551–1557, 2006.

[21] M. N. Melo, R. Ferre, and M. A. R. B. Castanho, “Antimicrobial peptides: linking partition, activity and high membrane-bound concentrations,” *Nat. Rev. Microbiol.*, vol. 7, pp. 245–250, 2009.

[22] M. R. Yeaman and N. Y. Yount, “Mechanisms of antimicrobial peptide action and resistance,” *Pharmacol. Rev.*, vol. 55, no. 1, pp. 27–55, 2003.

[23] Z. Oren and Y. Shai, “Mode of action of linear amphipathic alpha-helical antimicrobial peptides,” *Biopolymers*, vol. 47, pp. 451–463, 1998.

[24] N. Papo and Y. Shai, “Host defense peptides as new weapons in cancer treatment,” *Cell. Mol. Life Sci.*, vol. 62, pp. 784–790, 2005.

[25] H. Leontiadou, A. E. Mark, and S. J. Marrink, “Antimicrobial peptides in action,” *J. Am. Chem. Soc.*, vol. 128, pp. 12156–12161, 2006.

[26] D. Sengupta, H. Leontiadou, A. E. Mark, and S. J. Marrink, “Toroidal pores formed by antimicrobial peptides show significant disorder,” *Biochim. Biophys. Acta - Biomembr.*, vol. 1778, pp. 2308–2317, 2008.

[27] F. Harris, S. R. Dennison, J. Singh, and D. A. Phoenix, “On the selectivity and efficacy of defense peptides with respect to cancer cells,” *Med. Res. Rev.*, vol. 33, no. 1, pp. 190–234, 2013.

[28] F. Schweizer, “Cationic amphiphilic peptides with cancer-selective toxicity,” *Eur. J. Pharmacol.*, vol. 625, pp. 190–194, 2009.

[29] C. S. Alves, M. N. Melo, H. G. Franquelim, R. Ferre, M. Planas, L. Feliu, E. Bardají, W. Kowalczyk, D. Andreu, N. C. Santos, M. X. Fernandes, and M. A. R. B. Castanho, “Escherichia coli cell surface perturbation and disruption induced by antimicrobial peptides BP100 and pepR,” *J. Biol. Chem.*, vol. 285, no. 36, pp. 27536–27544, 2010.

[30] M. M. B. Ribeiro, M. M. Domingues, J. M. Freire, N. C. Santos, and M. A. R. B. Castanho, “Translocating the blood-brain barrier using electrostatics,” *Front. Cell. Neurosci.*, vol. 6, 2012.

[31] J. M. Freire, A. S. Veiga, I. Rego de Figueiredo, B. G. de la Torre, N. C. Santos, D. Andreu, A. T. Da Poian, and M. a R. B. Castanho, “Nucleic acid delivery by cell penetrating peptides derived from dengue virus capsid protein: design and mechanism of action.,” *FEBS J.*, vol. 281, pp. 191–215, 2014.

[32] J. M. Freire, M. M. Domingues, J. Matos, M. N. Melo, A. S. Veiga, N. C. Santos, and M. A. R. B. Castanho, “Using zeta-potential measurements to quantify peptide partition to lipid membranes,” *Eur. Biophys. J.*, vol. 40, pp. 481–487, 2011.

[33] A. Cederlund, G. H. Gudmundsson, and B. Agerberth, “Antimicrobial peptides important in innate immunity,” *FEBS J.*, vol. 278, pp. 3942–3951, 2011.

[34] J. Winter, A. Pantelis, D. Kraus, J. Reckenbeil, R. Reich, S. Jepsen, H.-P. Fischer, J.-P. Allam, N. Novak, and M. Wenghoefer, “Human alpha-defensin (DEFA) gene expression helps to characterise benign and malignant salivary gland tumours,” *BMC Cancer*, vol. 12, 2012.

[35] M. Nishimura, Y. Abiko, Y. Kurashige, M. Takeshima, M. Yamazaki, K. Kusano, M. Saitoh, K. Nakashima, T. Inoue, and T. Kaku, “Effect of defensin peptides on eukaryotic cells: Primary epithelial cells, fibroblasts and squamous cell carcinoma cell lines,” *J. Dermatol. Sci.*, vol. 36, pp. 87–95, 2004.

[36] J. Winter and M. Wenghoefer, “Human defensins: Potential tools for clinical applications,” *Polymers (Basel).*, vol. 4, no. 1, pp. 691–709, 2012.

[37] J. Jarczak, E. M. Kościuczuk, P. Lisowski, N. Strzałkowska, A. Jóźwik, J. Horbańczuk, J. Krzyzewski, L. Zwierzchowski, and E. Bagnicka, “Defensins: Natural component of human innate immunity,” *Hum. Immunol.*, vol. 74, pp. 1069–1079, 2013.

[38] Y. S. Wang, D. Li, H. S. Shi, Y. J. Wen, L. Yang, N. Xu, X. C. Chen, X. Chen, P. Chen, J. Li, H. X. Deng, C. T. Wang, G. Xie, S. Huang, Y. Q. Mao, L. J. Chen, X. Zhao, and Y. Q. Wei, “Intratumoral expression of mature human neutrophil peptide-1 mediates antitumor immunity in mice,” *Clin. Cancer Res.*, vol. 15, no. 22, pp. 6901–6911, 2009.

[39] S. T. W. McKeown, F. T. Lundy, J. Nelson, D. Lockhart, C. R. Irwin, C. G. Cowan, and J. J. Marley, “The cytotoxic effects of human neutrophil peptide-1 (HNP1) and lactoferrin on oral squamous cell carcinoma (OSCC) in vitro,” *Oral Oncol.*, vol. 42, pp. 685–690, 2006.

[40] E. Balducci, A. Bonucci, M. Picchianti, R. Pogni, and E. Talluri, “Structural and functional consequences induced by post-translational modifications in alpha-defensins,” *Int. J. Pept.*, vol. 2011, 2011.

[41] C. a Müller, J. Markovic-Lipkovski, T. Klatt, J. Gamper, G. Schwarz, H. Beck, M. Deeg, H. Kalbacher, S. Widmann, J. T. Wessels, V. Becker, G. a Müller, and T. Flad, “Human alpha-defensins HNPs-1, -2, and -3 in renal cell carcinoma: influences on tumor cell proliferation.,” *Am. J. Pathol.*, vol. 160, no. 4, pp. 1311–1324, 2002.

[42] D. Gaspar, J. M. Freire, T. R. Pacheco, J. T. Barata, and M. A. R. B. Castanho, “Apoptotic human neutrophil peptide-1 anti-tumor activity revealed by cellular biomechanics,” *Biochim. Biophys. Acta*, vol. 1853, pp. 308–316, 2014.

[43] a. Lichtenstein, “Mechanism of mammalian cell lysis mediated by peptide defensins: Evidence for an initial alteration of the plasma membrane,” *J. Clin. Invest.*, vol. 88, no. 1, pp. 93–100, 1991.

[44] P. D. Games, I. S. Dos Santos, E. O. Mello, M. S. S. Diz, A. O. Carvalho, G. A. de Souza-Filho, M. Da Cunha, I. M. Vasconcelos, B. D. S. Ferreira, and V. M. Gomes, “Isolation, characterization and cloning of a cDNA encoding a new antifungal defensin from Phaseolus vulgaris L. seeds.,” *Peptides*, vol. 29, pp. 2090–2100, 2008.

[45] Y.-F. Yang and P.-C. Lyu, “The proteins of plant defensin family and their application beyond plant disease control.,” *Recent Pat. DNA Gene Seq.*, vol. 2, no. 3, pp. 214–218, 2008.

[46] E. D. O. Mello, I. S. dos Santos, A. D. O. Carvalho, L. S. de Souza, G. a de Souza-Filho, V. V do Nascimento, O. L. T. Machado, U. Zottich, and V. M. Gomes, “Functional expression and activity of the recombinant antifungal defensin PvD1r from Phaseolus vulgaris L. (common bean) seeds.,” *BMC Biochem.*, vol. 15, no. 7, 2014.

[47] W. F. Broekaert, F. R. Terras, B. P. Cammue, and R. W. Osborn, “Plant defensins: novel antimicrobial peptides as components of the host defense system.,” *Plant Physiol.*, vol. 108, pp. 1353–1358, 1995.

[48] E. O. Mello, S. F. F. Ribeiro, A. O. Carvalho, I. S. Santos, M. Da Cunha, C. Santa-Catarina, and V. M. Gomes, “Antifungal activity of PvD1 defensin involves plasma membrane permeabilization, inhibition of medium acidification, and induction of ROS in fungi cells,” *Curr. Microbiol.*, vol. 62, pp. 1209–1217, 2011.

[49] M. H. Ross and W. Pawlina, “Tissues: Concept and Classification,” in *Histology: a text and atlas: with correlated cell and molecular biology*, 6th ed., M. H. Ross and W. Pawlina, Eds. Lippincott Williams & Wilkins, 2011, pp. 98–101.

[50] R. A. Weinberg, “The Nature of Cancer,” in *The Biology of Cancer*, 2nd ed., E. Zayatz and R. K. Mickey, Eds. New York: Garland Science, Taylor & Francis Group, 2014, pp. 31–50.

[51] G. Bendas and L. Borsig, “Cancer cell adhesion and metastasis: Selectins, integrins, and the inhibitory potential of heparins,” *Int. J. Cell Biol.*, vol. 2012, 2012.

[52] A. Magarkar, V. Dhawan, P. Kallinteri, T. Viitala, M. Elmowafy, T. Róg, and A. Bunker, “Cholesterol level affects surface charge of lipid membranes in saline solution,” *Sci. Rep.*, vol. 4, 2014.

[53] J. S. Mader and D. W. Hoskin, “Cationic antimicrobial peptides as novel cytotoxic agents for cancer treatment,” *Expert Opin. Investig. Drugs*, vol. 15, no. 8, pp. 933–946, 2006.

[54] N. M. Goldenberg and B. E. Steinberg, “Surface charge: A key determinant of protein localization and function,” *Cancer Res.*, vol. 70, no. 4, pp. 1277–1280, 2010.

[55] R. A. Weinberg, “p53 and Apoptosis: Master Guardian and Executioner ,” in *The Biology of Cancer*, 2nd ed., E. Zayatz and R. K. Mickey, Eds. New York: Garland Science, Taylor & Francis Group, 2014, pp. 361–363.

[56] F. Vural, S. Cebesoy, and M. Karakas, “Classification of Cell Death,” *J. Entomol. Zool. Stud.*, vol. 1, no. 5, pp. 120–126, 2013.

[57] G. M. Suarez-Jimenez, A. Burgos-Hernandez, and J. M. Ezquerra-Brauer, “Bioactive peptides and depsipeptides with anticancer potential: Sources from marine animals,” *Mar. Drugs*, vol. 10, pp. 963–986, 2012.

[58] M. Girasole, A. Cricenti, R. Generosi, G. Longo, G. Pompeo, S. Cotesta, and A. Congiu-Castellano, “Different membrane modifications revealed by atomic force/lateral force microscopy after doping of human pancreatic cells with Cd, Zn, or Pb,” *Microsc. Res. Tech.*, vol. 70, pp. 912–917, 2007.

[59] L. Kupcsik, “Estimation of Cell Number Based on Metabolic Activity: The MTT Reduction Assay,” in *Mammalian Cell Viability Methods and Protocols*, M. J. Stoddart, Ed. Switzerland: Human Press - Springer, 2011, pp. 13–15.

[60] T. L. Riss, R. A. Moravec, A. L. Niles, H. A. Benink, T. J. Worzella, and L. Minor, “Cell Viability Assays,” *NCBI Books*. [Online]. Available: http://www.ncbi.nlm.nih.gov/books/NBK144065/?report=reader. [Accessed: 07-May-2015].

[61] G. Nikkhah, J. C. Tonn, O. Hoffmann, H.-P. Kraemer, J. L. Darling, W. Schachenmayr, and R. Schönmayr, “The MTT assay for chemosensitivity testing of human tumors of the central nervous system,” *J. Neurooncol.*, vol. 13, pp. 1–11, 1992.

[62] T. Bernas and J. Dobrucki, “Mitochondrial and nonmitochondrial reduction of MTT: Interaction of MTT with TMRE, JC-1, and NAO mitochondrial fluorescent probes,” *Cytometry*, vol. 47, pp. 236–242, 2002.

[63] Y. Liu, D. A. Peterson, H. Kimura, and D. Schubert, “Mechanism of Cellular 3-(4,5-Dimethylthiazol-2-yl) -2,5- Diphenyltetrazolium Bromide (MTT) Reduction,” *J. Neurochem. Lippincott—Raven Publ.*, vol. 69, no. 2, pp. 581–593, 1997.

[64] M. M. Domingues and N. C. Santos, “Laser-Light Scattering Approach to Peptide–Membrane Interaction,” in *Membrane Active Peptides: Methods and Results on Structure and Function*, 1st ed., M. A. R. B. Castanho, Ed. International University Line, 2009, pp. 146–160.

[65] A. Sze, D. Erickson, L. Ren, and D. Li, “Zeta-potential measurement using the Smoluchowski equation and the slope of the current-time relationship in electroosmotic flow,” *J. Colloid Interface Sci.*, vol. 261, pp. 402–410, 2003.

[66] Malvern Instruments, “Zeta potential - An introduction in 30 minutes.” pp. 1–6, 2011.

[67] M. M. Domingues, P. S. Santiago, M. A. R. B. Castanho, and N. C. Santos, “What can light scattering spectroscopy do for membrane-active peptide studies?,” *J. Pept. Sci.*, vol. 14, pp. 394–400, 2008.

[68] R. Marsalek, “Zeta Potential - Applications,” in *International Conference on Environment and Industrial Innovation*, 2012, vol. 35, pp. 15–19.

[69] G. Binnig, C. F. Quate , E. L. Gi, and C. Gerber, “Atomic Force Microscope,” *Phys. Rev. Lett.*, vol. 56, no. 9, pp. 930–933, 1986.

[70] P. Eaton and P. West, Eds., “Introduction,” in *Atomic Force Microscopy*, 1st ed., New York: Oxford University Press Inc, 2010, pp. 1–2.

[71] N. C. Santos and M. A. R. B. Castanho, “An overview of the biophysical applications of atomic force microscopy,” *Biophys. Chem.*, vol. 107, pp. 133–149, 2004.

[72] D. J. Müller and Y. F. Dufrêne, “Atomic force microscopy: A nanoscopic window on the cell surface,” *Trends Cell Biol.*, vol. 21, no. 8, pp. 461–469, 2011.

[73] R. Benitez and J. E. L. Toca-Herrera, “Looking at Cell Mechanics with Atomic Force Microscopy: Experiment and Theory,” *Microsc. Res. Tech.*, vol. 77, pp. 947–958, 2014.

[74] T. G. Kuznetsova, M. N. Starodubtseva, N. I. Yegorenkov, S. A. Chizhik, and R. I. Zhdanov, “Atomic force microscopy probing of cell elasticity,” *Micron*, vol. 38, pp. 824–833, 2007.

[75] D. Fuoco, “A New Method for Characterization of Natural Zeolites and Organic Nanostructure Using Atomic Force Microscopy,” *Nanomaterials*, vol. 2, pp. 79–91, 2012.

[76] P. Eaton and P. West, Eds., “AFM modes,” in *Atomic Force Microscopy*, 1st ed., New York: Oxford University Press Inc., 2010, pp. 49–55.

[77] “JPK Tutorials - Atomic Force Microscopy (AFM),” *Introduction to Imaging modes*. [Online]. Available: http://usa.jpk.com/introduction-to-imaging-modes.433.us.html. [Accessed: 05-Jun-2015].

[78] R. Barattin and N. Voyer, “Chemical modifications of AFM tips for the study of molecular recognition events,” *Chem. Commun. (Camb).*, no. 13, pp. 1513–1532, 2008.

[79] Y. F. Dufrêne, “Sticky microbes: forces in microbial cell adhesion,” *Trends Microbiol.*, vol. 23, no. 6, pp. 376–382, 2015.

[80] Y. F. Dufrêne, D. Martínez-Martín, I. Medalsy, D. Alsteens, and D. J. Müller, “Multiparametric imaging of biological systems by force-distance curve–based AFM,” *Nat. Methods*, vol. 10, pp. 847–854, 2013.

[81] P. Eaton and P. West, “Applications of AFM,” in *Atomic Force Microscopy*, 1st ed., P. Eaton and P. West, Eds. New York: Oxford University Press Inc., 2010, pp. 139–142.

[82] “MCF 10A (ATCC® CRL-10317™),” *ATCC*. [Online]. Available: http://www.lgcstandards-atcc.org/products/all/CRL-10317.aspx?geo_country=pt. [Accessed: 10-Dec-2014].

[83] “MDA-MB-231 (ATCC® HTB-26™),” *ATCC*. [Online]. Available: http://www.lgcstandards-atcc.org/products/all/HTB-26.aspx?geo_country=pt. [Accessed: 12-Sep-2014].

[84] D. B. Agus and et al, “A physical sciences network characterization of non-tumorigenic and metastatic cells.,” *Sci. Rep.*, vol. 3, pp. 1–12, 2013.

[85] I. R. De Figueiredo, J. M. Freire, L. Flores, A. S. Veiga, and M. A. R. B. Castanho, “Cell-penetrating peptides: A tool for effective delivery in gene-targeted therapies,” *IUBMB Life*, vol. 66, no. 3, pp. 182–194, 2014.

[86] A. Lichtenstein, T. Ganz, M. E. Selsted, and R. I. Lehrer, “In Vitro Tumor Cell Cytolysis Mediated by Peptide Defensins of Human and Rabbit Granulocytes,” *Blood J.*, vol. 68, no. 6, pp. 1407–1410, 1986.

[87] Y. Zhang, M. Yang, N. G. Portney, D. Cui, G. Budak, E. Ozbay, M. Ozkan, and C. S. Ozkan, “Zeta potential: A surface electrical characteristic to probe the interaction of nanoparticles with normal and cancer human breast epithelial cells,” *Biomed. Microdevices*, vol. 10, pp. 321–328, 2008.

[88] G. M. Cook and W. Jacobson, “The electrophoretic mobility of normal and leukaemic cells of mice.,” *Biochem. J.*, vol. 107, pp. 549–557, 1968.

[89] E. Severi, D. W. Hood, and G. H. Thomas, “Sialic acid utilization by bacterial pathogens,” *Microbiology*, vol. 153, pp. 2817–2822, 2007.

[90] N. Tatsumi, I. Tsuda, M. Masaoka, and K. Imai, “Measurement of the zeta potential of human platelets by the use of laser-light scattering,” *Thromb. Res.*, vol. 65, pp. 585–592, 1992.

[91] M. M. B. Ribeiro, A. R. T. Pinto, M. M. Domingues, I. Serrano, M. Heras, E. R. Bardaji, I. Tavares, and M. A. Castanho, “Chemical conjugation of the neuropeptide kyotorphin and ibuprofen enhances brain targeting and analgesia,” *Mol. Pharm.*, vol. 8, no. 5, pp. 1929–1940, 2011.

[92] D. Gaspar, A. S. Veiga, C. Sinthuvanich, J. P. Schneider, and M. A. R. B. Castanho, “Anticancer peptide SVS-1: Efficacy precedes membrane neutralization,” *Biochemistry*, vol. 51, pp. 6263–6265, 2012.

[93] K. Shahidullah and E. London, “Effect of lipid composition on the topography of membraneassociated hydrophobic helices: stabilization of transmembrane topography by anionic lipids,” *J. Membr Biol*, vol. 379, no. 4, pp. 704–718, 2008.

[94] J. Shankar, A. Messenberg, J. Chan, T. M. Underhill, L. J. Foster, and I. R. Nabi, “Pseudopodial actin dynamics control epithelial-mesenchymal transition in metastatic cancer cells,” *Cancer Res.*, vol. 70, no. 9, pp. 3780–3790, 2010.

[95] P. D Antonio, M. Lasalvia, G. Perna, and V. Capozzi, “Scale-independent roughness value of cell membranes studied by means of AFM technique,” *Biochim. Biophys. Acta - Biomembr.*, vol. 1818, pp. 3141–3148, 2012.

[96] M. Girasole, G. Pompeo, A. Cricenti, G. Longo, G. Boumis, A. Bellelli, and S. Amiconi, “The how, when, and why of the aging signals appearing on the human erythrocyte membrane: An atomic force microscopy study of surface roughness,” *Nanomedicine Nanotechnology, Biol. Med.*, vol. 6, pp. 760–768, 2010.

[97] R. Kaul-Ghanekar, S. Singh, H. Mamgain, A. Jalota-Badhwar, K. M. Paknikar, and S. Chattopadhyay, “Tumor suppressor protein SMAR1 modulates the roughness of cell surface: combined AFM and SEM study.,” *BMC Cancer*, vol. 9, 2009.